Contrib Mineral Petrol (2015) 169:47
DOI 10.1007/s00410-015-1143-6

ORIGINAL PAPER

Timing and conditions of metamorphism and melt crystallization in Greater Himalayan rocks, eastern and central Bhutan: insight from U–Pb zircon and monazite geochronology and trace-element analyses

K. Zeiger[1] · S. M. Gordon[1] · S. P. Long[2] · A. R. C. Kylander-Clark[3] · K. Agustsson[1] · M. Penfold[1]

Received: 22 November 2014 / Accepted: 17 April 2015

Abstract Within the eastern Himalaya in central and eastern Bhutan, Greater Himalayan (GH) rocks are interpreted to have been thickened by the Kakhtang thrust (KT). In order to understand the metamorphic and exhumation history of the GH and to evaluate the structural significance of the KT, zircon and monazite from twenty samples were analyzed by laser-ablation split-stream ICPMS. In eastern Bhutan, zircon and monazite from samples collected in the KT hanging wall revealed ca. 36–28 Ma metamorphism. Subsequently, the initiation of melt crystallization shows a trend with structural distance above the KT, with early melt crystallization (ca. 27 Ma) in the structurally highest samples and younger melt crystallization (ca. 16 Ma) for leucosomes within the KT zone. Melt crystallization was protracted and continued until ca. 14–13 Ma in both the KT hanging wall and the footwall. In comparison, in central Bhutan, two leucosomes revealed extended melt crystallization from ca. 31 to 19 Ma. The youngest zircon dates from samples exposed structurally above and below the KT are similar, indicating that the KT was not as significant of a structure as other fault systems to which it has been correlated. However, the younging trend in the initiation of melt crystallization with decreasing structural distance above the KT argues that progressive underplating of ductile material assisted in the initial emplacement of the GH unit in central and eastern Bhutan. The KT likely represents a minor shear zone that aided in this underplating process.

Keywords Himalaya · Bhutan · Greater Himalayan rocks · Zircon · Split-stream LA-ICPMS

Communicated by Othmar Müntener.

Electronic supplementary material The online version of this article (doi:10.1007/s00410-015-1143-6) contains supplementary material, which is available to authorized users.

✉ S. M. Gordon
staciag@unr.edu

[1] Department of Geological Sciences, University of Nevada, Reno, NV, USA

[2] Nevada Bureau of Mines and Geology, University of Nevada, Reno, NV, USA

[3] Earth Research Institute, University of California, Santa Barbara, CA, USA

Introduction

High-grade, ductile metamorphic rocks represent the supporting base for orogenic belts during crustal thickening and growth. Within some active orogenic belts, and in many ancient orogens that have undergone collapse, these high-grade rocks typically show evidence of lateral flow and potentially extrusion from mid- to lower-crustal depths to the near surface (e.g., Royden et al. 1997; Beaumont et al. 2001; Vanderhaeghe and Teyssier 2001; Torvela et al. 2013). Understanding the pressure–temperature–time evolution of these rocks—from their burial to their emplacement near the surface—can provide insight into the metamorphic and deformational processes that control the evolution of orogenic belts (e.g., England and Thompson 1984; Pyle and Spear 2003; Stearns et al. 2013).

The Himalaya is considered the type example of an active continent–continent collisional orogen (e.g., LeFort 1975; Hodges 2000; Yin 2006), and it formed due to collision and continued convergence between the Indian and Eurasian plates that began at ca. 50 Ma (e.g., Rowley 1996; Ding et al. 2005; Leech et al. 2005; Najman et al. 2010). Convergence has resulted in the burial and metamorphism

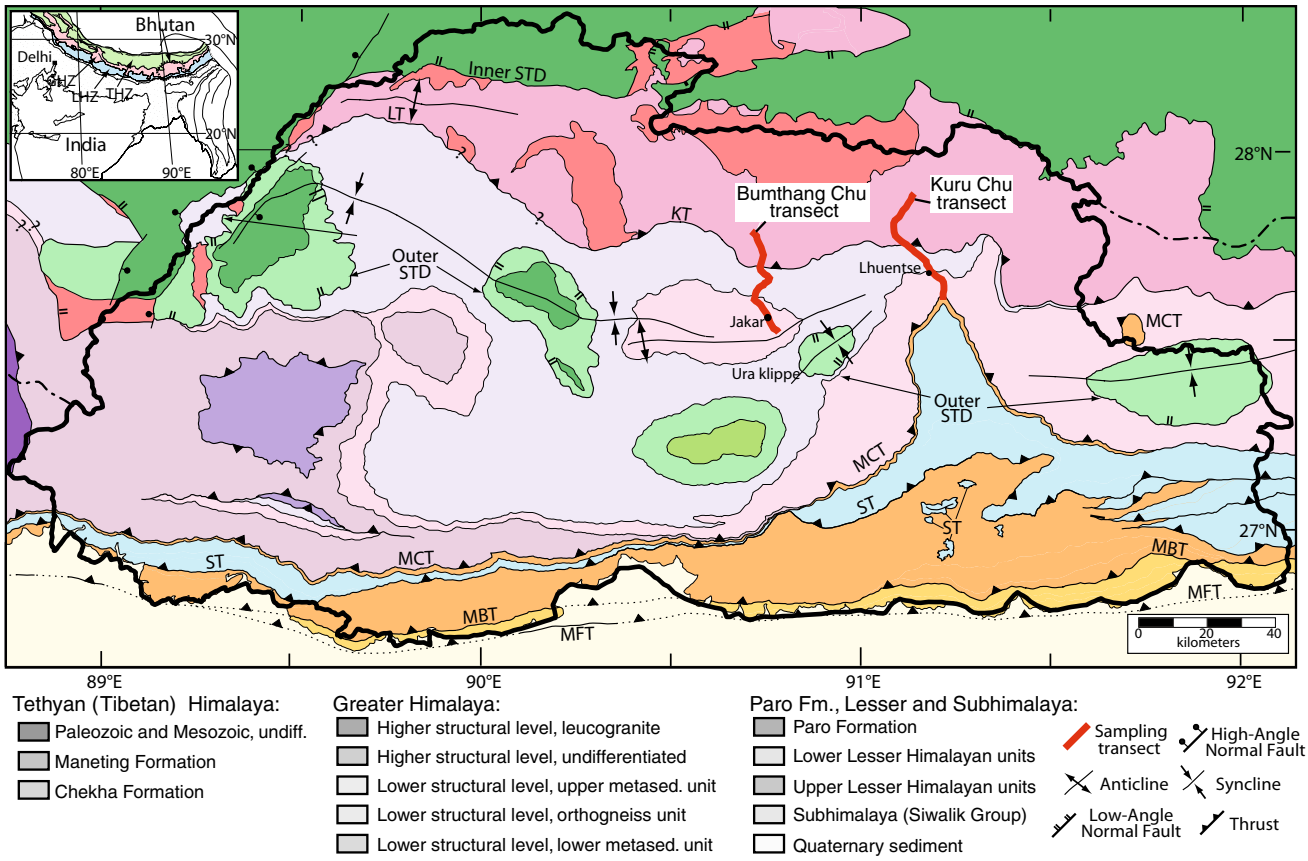

Fig. 1 Simplified geologic map showing major lithologic and structural units of Bhutan and surrounding regions, modified from Long et al. (2012). Transects from this study are in highlighted in red. Inset: major lithologic units and geographic location of Bhutan within the Himalaya. *STD* South Tibetan detachment, *KT* Kakhtang thrust, *LT* Laya thrust, *MCT* Main Central thrust, *ST* Shumar thrust, *MBT* Main Boundary thrust, *MFT* Main Frontal thrust, *THZ* Tethyan Himalayan zone, *GH* Greater Himalayan zone, *LH* Lesser Himalayan rocks

of a composite series of sedimentary basins that had once covered the northern margin of India (e.g., Molnar 1984; Mattauer 1986; Hodges 2000; Yin and Harrison 2000; DeCelles et al. 2002). These rocks have been translated southward and structurally imbricated, forming the Himalayan fold–thrust belt and producing significant crustal thickening and several kilometers of topographic uplift (e.g., Molnar 1984). Within the hinterland of the fold–thrust belt, some of these sedimentary rocks are currently exposed as a thick section of exhumed mid- to lower-crustal rocks, referred to here as the Greater Himalayan (GH) rocks (e.g., Gansser 1964; Hodges 2000; Yin 2006).

Across much of the eastern Himalaya, the GH is structurally thickened and divided into two units by an intra-GH shear zone (Gansser 1983; Swapp and Hollister 1991; Yin et al. 2006; Chakungal et al. 2010; Warren et al. 2011a; 2014). Within the central and eastern part of the kingdom of Bhutan, the Kakhtang thrust (KT) separates the GH into structurally higher (upper-GH) and structurally lower levels (lower-GH) (Fig. 1; Grujic et al. 2002). Multiple studies have investigated the petrologic, structural, and protolith history of the lower-GH, revealing evidence for upper amphibolite-facies to upper greenschist-facies peak metamorphic conditions (Davidson et al. 1997; Daniel et al. 2003; Corrie et al. 2012), with minimal evidence for partial melting in the upper part of the unit (Long and McQuarrie 2010).

In contrast, in the upper-GH in central and eastern Bhutan, field observations suggest overall higher-grade metamorphic conditions in comparison with the lower-GH. Some of the upper-GH rocks may have crossed the second sillimanite isograd, and there is a higher volume percentage of crystallized melt exposed in the form of migmatites and crosscutting dikes found in outcrops throughout the unit, as well as in regional-scale leucogranite bodies (e.g., Swapp and Hollister 1991; Grujic et al. 2002). Because the presence of a small amount (>7 vol%) of melt can lead to a drastic reduction in the strength of rocks (Rosenberg and Handy 2005), it is important to understand the timing and conditions under which melting began and crystallized (e.g., Jamieson et al. 2011), as well as the timing and conditions of metamorphism and deformation.

This investigation presents new laser-ablation split-stream inductively coupled plasma mass spectrometry (LASS-ICPMS) zircon and monazite geochronology and trace-element analyses from twenty pelitic, leucocratic, and gneissic samples collected along two transects through the GH that cross the KT in central and eastern Bhutan. The data were collected to constrain the timing of melt crystallization and metamorphism across the unit and are used to evaluate the driving mechanisms for exhumation of the GH rocks and the role of the KT in the history of the eastern Himalaya.

Geologic setting

Himalayan orogenic belt

The Himalayan orogenic belt consists of four main tectonostratigraphic zones that are exposed parallel to the strike of the orogen (e.g., Gansser 1964; LeFort 1975; Hodges 2000; Yin 2006). From north to south, the units include the Tethyan Himalayan rocks, the GH rocks, the Lesser Himalayan rocks (LH), and the SubHimalayan rocks (Fig. 1). The Tethyan Himalaya is comprised of low-grade to unmetamorphosed sedimentary rocks that were originally deposited in the early Paleozoic–early Tertiary southern passive-margin basin of the Tethyan Ocean (e.g., Gaetani and Garzanti 1991; Garzanti 1999; Yin and Harrison 2000). Tethyan Himalayan rocks are juxtaposed against GH rocks across the South Tibetan detachment (STD), a system of top-to-the-north shear zones and normal faults (Burchfiel et al. 1992; Hodges 2000). The GH dominantly consists of (upper)amphibolite-facies, locally granulite-facies, orthogneiss, and metasedimentary rocks, which typically show evidence for having undergone melting during Himalayan orogenesis (e.g., Gansser 1964; Harrison et al. 1997, 1998; Hodges 2000). In addition, large Miocene leucogranite intrusions are exposed within the GH (Hodges 2000).

The GH structurally overlies the LH, which consists of Paleoproterozoic to Permian greenschist-facies to unmetamorphosed sedimentary rocks (e.g., Yin 2006; Myrow et al. 2009; Kohn et al. 2010; Long et al. 2011a; Martin et al. 2011) that have been deformed into a south-vergent fold–thrust belt (e.g., Schelling and Arita 1991a, b; Srivastava and Mitra 1994; Robinson et al. 2006; Mitra et al. 2010; Long et al., 2011b). The Main Central thrust (MCT), a top-to-the-south-sense ductile shear zone, separates these two zones (Heim and Gansser 1939; Gansser 1964, 1983; Grujic et al. 2002; Yin 2006). Finally, the SubHimalayan rocks represent sediments deposited in the syn-orogenic, Neogene–Quaternary foreland basin that subsided south of the Himalayan orogenic belt. They are now juxtaposed structurally below the LH across the Main Boundary thrust and are bound at their base by the Main Frontal thrust, which represents the modern Himalayan deformation front (e.g., Gansser 1964; Burbank et al. 1996; DeCelles et al. 1998; 2004; Huyghe et al. 2005).

Bhutan: the eastern Himalaya

While these four tectonostratigraphic zones are present in Bhutan, this part of the eastern Himalaya reveals some distinct structural features, including, in central and eastern Bhutan, the Kakhtang thrust (KT; Fig. 1), which divides the GH into the upper- and lower-GH structural units (Fig. 1; Gansser 1983; Swapp and Hollister 1991; Bhargava 1995; Grujic et al. 2002; Daniel et al. 2003). The KT has been interpreted to correlate with the Laya thrust in northwest Bhutan (Grujic et al. 2011; Long et al. 2011c; Warren et al. 2011a, b) and the Zimithang thrust to the east within Arunachal Pradesh (Yin et al. 2006, 2010a, b; Warren et al. 2014), and previous investigations have proposed that these thrust systems are out-of-sequence with respect to the structurally lower MCT.

The Bhutan Himalaya also contains multiple exposures of the STD (Fig. 1). The inner STD (Kellett et al. 2009), farther to the hinterland of the orogen, represents the primary exposure of the fault system found across much of the Himalaya. The inner STD juxtaposes Tethyan Himalayan rocks against the GH, and in Bhutan, more specifically the upper-GH. In comparison, the outer STD (Kellett et al. 2009) is exposed closer to the orogenic front and separates isolated Tethyan sedimentary rocks from the lower-GH (e.g., Grujic et al. 2002). Four of these Tethyan exposures are interpreted as Klippen above ductile, normal-sense shear zones (Kellett et al. 2010), whereas an exposure in south-central Bhutan has been interpreted to represent an intact depositional sequence from the lower-GH through Tethyan Himalayan rocks (Fig. 1; Long and McQuarrie 2010; Corrie et al. 2012).

Limited geochronologic data place constraints on the timing of the structures that bound the upper-GH. By ca. 16 Ma, monazite from leucogranite within the outer STD zone had crystallized (Kellett et al. 2010). Subsequently, deformation is interpreted to have shifted to higher structural levels, initiating coeval movement on the KT and inner STD at ca. 16 Ma in central and eastern Bhutan (Grujic et al. 2002; Daniel et al. 2003; Kellett et al. 2009). The inner STD continued to be active until at least ca. 11 Ma (Edwards and Harrison 1997; Wu et al. 1998; Kellett et al. 2009). Therefore, Grujic et al. (2002) postulated that the KT and inner STD were concurrently active from ca. 16 to 11 Ma.

GH units

The majority of the upper-GH, located in the hanging wall of the KT and below the inner STD in central and eastern

Bhutan (Fig. 1), is composed of upper amphibolite-facies orthogneiss, metasedimentary rocks, and Miocene granite intrusions (Gansser 1983; Swapp and Hollister 1991; Davidson et al. 1997; Grujic et al. 1996, 2002; Daniel et al. 2003; Long et al. 2011b, c), although no published quantitative estimates of peak metamorphic pressures and temperatures have been described from these rocks. Grujic et al. (1996) presented a single deformation temperature estimate between ca. 650 and 750 °C from a leucogranite dike injected into the KT zone. In addition, sparse geochronologic data exist for the upper-GH in central and eastern Bhutan. The only existing date is from a dike within the KT zone, which was interpreted to limit the maximum timing of movement on the KT to ca. 15–14 Ma (Grujic et al. 2002; Daniel et al. 2003).

Most of the structural, petrologic, and geochronometric work on the Bhutan upper-GH has been concentrated in the region exposed above the Laya thrust in western Bhutan (Fig. 1). In addition to gneiss and granite, rare granulitized eclogites, found in northwestern Bhutan and also to the west in the Arun Valley in eastern Nepal and the Ama Drime Range in southern Tibet, revealed that these rocks achieved eclogite-facies conditions of ≥14 kbar/580 °C at ca. 21–14 Ma, followed by a granulite-facies overprint of 7–12 kbar/750–800 °C at ca. 14–13 Ma (Groppo et al. 2007; Cottle et al. 2009; Corrie et al. 2010; Grujic et al. 2011; Warren et al. 2011a). In addition, migmatitic gneisses, leucosomes, and granite have yielded crystallization ages of ca. 16–11 Ma (zircon; Kellett et al. 2009) and ca. 15–13 Ma (monazite; Edwards and Harrison 1997; Warren et al. 2011b) from the upper-GH in western Bhutan. $^{40}Ar/^{39}Ar$ muscovite cooling ages from just north of the western Bhutan border suggest that the upper-GH experienced rapid cooling and exhumation by ca. 11–10 Ma (Maluski et al. 1988).

Structurally below the KT, the lower-GH is composed of orthogneiss and metasedimentary rocks. In easternmost Bhutan, these rocks experienced peak pressures that increase structurally upward from 8–12 kbar/650–700 °C just above the MCT to 10–14 kbar/750–800 °C in the middle of the unit (Daniel et al. 2003). These rocks subsequently followed a near-isothermal decompression path to 4–6 kbar (Swapp and Hollister 1991; Davidson et al. 1997). Non-migmatitic rocks just below the KT in east–central Bhutan revealed lower-grade conditions of 600 °C/8 kbar (Davidson et al. 1997). Finally, in south-central Bhutan, the lower-GH experienced peak temperatures of ~650–700 °C at ~10–11 kbar in migmatitic rocks just above the MCT, and the P–T conditions decrease moving structurally higher in the unit to 550–600 °C at 7–9 kbar in non-migmatitic rocks at the top of the lower-GH (Corrie et al. 2012).

In regard to the timing of lower-GH metamorphism, in western Bhutan, monazite associated with sillimanite-facies metamorphism yielded dates of 21–17 Ma (Warren et al. 2011b), whereas monazite from western Bhutan granite crystallized nearly coevally between ca. 24 and 18 Ma (Carosi et al. 2006). In central Bhutan, a kyanite-bearing schist within the lower-GH below the Ura klippe (Fig. 1) yielded dates from monazite included in garnet and kyanite at ca. 26–21 Ma, indicating the timing of prograde metamorphism, and ca. 20–15 Ma from matrix monazite, interpreted as dating peak metamorphic conditions (Kellett et al. 2010). Moving farther east, monazite from a schist just above the MCT was interpreted to record prograde metamorphism from ca. 24 to 22 Ma (Daniel et al. 2003), and in the same area, monazite and xenotime dates from lower-GH leucogranite revealed crystallization ages between ca. 18 and 14 Ma near the MCT, decreasing to ca. 13.5 Ma in the middle of the lower-GH (Daniel et al. 2003).

Previous studies have interpreted the lower-GH as a ductile channel, bounded below by the MCT and above by the outer STD (Grujic et al. 1996, 2002; Hollister and Grujic 2006; Kellett et al. 2009). However, Long and McQuarrie (2010) found that the magnitude of channel-type flow within the lower-GH in central Bhutan is small, only representing 12–15 % of the total amount of shortening recorded in the Himalayan thrust belt in Bhutan. This, combined with a petrologic study that did not show evidence for a major decrease in P–T conditions across the structural level that had previously been mapped as the outer STD (Corrie et al. 2012), was used to argue that large-scale channel flow was unlikely in the lower-GH.

Methods

Twenty samples were collected along the Kuru Chu and Bumthang Chu in northeast and north-central Bhutan (Fig. 1), respectively, in order to determine the age variation in melt crystallization and metamorphism across two transects from the lower-GH, across the KT, and into the upper-GH (Table 1). Zircon was extracted from nine metasedimentary samples, eight layer-parallel leucosomes, one crosscutting pegmatite, and two orthogneiss samples (Table 1) using standard mineral separation techniques at the University of Nevada, Reno. In addition, monazite was obtained from three of the metasedimentary rocks and one of the foliation-parallel leucosomes. Standard one-inch grain mounts were prepared, and cathodoluminescence (CL) and backscatter electron (BSE) images were obtained using the FEI Quanta 400f scanning electron microscope (SEM) at UC Santa Barbara for zircon and monazite, respectively. The images revealed internal zonation that was used to guide the LA-ICPMS analyses. The UC Santa Barbara ICPMS facility consists of a *Nu Plasma* multicollector-ICPMS (MC-ICPMS), a *Nu AttoM* single-collector-ICPMS,

Table 1 Studied metasedimentary, orthogneiss, and leucocratic samples from central and eastern Bhutan

Sample number	location	Distance above MCT (km)[a]	Distance above KT (km)	Rock Type	Mineral Assemblage[b]	Eocene to Miocene dates (Ma)[c]	Trace-element zircon trend	Ti-in-zircon temperature[d] (°C)	Ti phase
BU12-172c	Kuru Chu LH	−0.2	−6.9	Schist	Qz, Pl, Bt, Ms, Grt	*z*: 20.6 ± 0.4–16.8 ± 0.3	Decrease in HREE with decreasing age		
BU12-178c	Kuru Chu lower-GH	2.1	−4.6	Schist	Qz, Pl, Bt, Ms, Grt	*z*: inherited; *m*: 15.0 ± 0.5			
BU12-182	Kuru Chu lower-GH	3.5	−3.2	Metapelite	Qz, Pl, Bt, Ms, Grt, Ky	*z*: inherited; *m*: 16.9 ± 0.6–15.2 ± 0.6			
BU12-190a	Kuru Chu lower-GH	6.5	−0.2	Foliation-parallel leucosome	Qz, Pl, Bt, Grt	*z*: inherited; *m*: 14.1 ± 0.6–15.2 ± 0.6			
BU12-190b	Kuru Chu lower-GH	6.5	−0.2	Paragneiss	Qz, Pl, Bt, Ms, Grt, Tur	*z*: inherited			
BU12-193a	Kuru Chu lower-GH	6.7	0	Metapelite	Qz, Pl, Bt, Ms, Grt, Sil	*z*: 16.3 ± 0.5–14.5 ± 0.4; *m*: 15.2 ± 0.5–14.4 ± 0.5	No correlation	~565–680	ru, ilm
BU12-195a	Kuru Chu upper-GH	6.8	0.1	Foliation-parallel leucosome	Qz, Pl, Bt	*z*: 15.6 ± 0.3–12.7 ± 0.3	Increase in HREE steepness with decreasing age	~550–620	spn
BU12-200a	Kuru Chu upper-GH	7.4	0.7	Foliation-parallel leucosome	Qz, Pl, Bt	*z*: 20.9 ± 0.3–13.3 ± 0.2	No correlation		
BU12-200b	Kuru Chu upper-GH	7.4	0.7	Foliation-parallel leucosome	Qz, Pl, Ms, Bt	*z*: 24.5 ± 0.5–17.3 ± 0.3	No correlation		
BU12-205	Kuru Chu upper-GH	9.9	3.2	Foliation-parallel leucosome	Qz, Pl, Ms, Bt	*z*: 25.9 ± 1.1–19.2 ± 0.4	Oldest, ca. 26 and 22 ma, grains have flat HREE pattern	~530–710	ilm
BU12-207a	Kuru Chu upper-GH	10.6	3.9	Metapelite	Qz, Pl, Bt, Ms, Grt, Sil	*z*: 36.5 ± 0.8–28.1 ± 0.6	No correlation		
BU12-207b	Kuru Chu upper-GH	10.6	3.9	Foliation-parallel leucosome	Qz, Pl, Bt, Ms	*z*: 27.2 ± 0.8–13.9 ± 0.4	Increase in HREE steepness with decreasing age		
BU12-209	Kuru Chu upper-GH	11.5	4.8	Crosscutting pegmatite	Qz, Pl, Bt	*z*: 26.6 ± 0.6–17.3 ± 0.4	No correlation	~510–700	spn
BU12-221	Kuru Chu upper-GH	14	7.3	Orthogneiss	Qz, Pl, Bt, Ms, Grt, Sil	*z*: 27.8 ± 0.6, 23.0 ± 0.4	No correlation		
BU13-01b	Bumthang Chu lower-GH	3.4	−5.2	Metapelite	Qz, Pl, Bt, Ms, Grt, Ky	*z*: 30.2 ± 0.7–22.2 ± 0.5	No correlation	~540–670	ilm

Table 1 continued

Sample number	location	Distance above MCT (km)[a]	Distance above KT (km)	Rock Type	Mineral Assemblage[b]	Eocene to Miocene dates (Ma)[c]	Trace-element zircon trend	Ti-in-zircon temperature[d] (°C)	Ti phase
BU13-04b	Bumthang Chu lower-GH	5.3	3.3	Metapelite	Qz, Pl, Bt, Ms, Grt, Sil	*z*: 33.3 ± 0.8–20.7 ± 0.5	No correlation	~510–670	ilm
BU13-18b	Bumthang Chu lower-GH	7.7	0.9	Metapelite	Qz, Pl, Bt, Ms, St, Sil	*z*: 32.9 ± 0.7	No correlation	~590	ilm
BU13-23d	Bumthang Chu upper-GH	8.7	0.1	Foliation-parallel leucosome	Qz, Pl, Ms, Grt	*z*: 28.1 ± 0.7–14.0 ± 0.4	Youngest, ca. 14 ma grain had flat HREE pattern	~500–680	ilm
BU13-37b	Bumthang Chu upper-GH	11	2.4	Foliation-parallel leucosome	Qz, Pl, Kfs, Bt	*z*: 25.8 ± 0.7–17.9 ± 0.4	Increase in HREE steepness with decreasing age	~500–650	
BU13-42b	Bumthang Chu upper-GH	11.8	3.2	Orthogneiss	Qz, Pl, Bt, Amp, Grt	*z*: inherited			

[a] The MCT is defined in Long et al. (2011a, b, c), Daniel et al. (2003) and Davidson et al. (1997) as the structurally upsection transition from garnet-bearing schist of the Jaishidanda Formation rocks to rocks that contain leucosomes and an aluminosilicate

[b] Mineral abbreviations after Whitney and Evans (2010)

[c] z: zircon; m: monazite

[d] Ti was only measured in samples that were dated on the second trip to UC Santa Barbara when a quadrupole ICPMS was used for the trace-element measurements. Temperatures calculated using the calibration of Watson et al. (2006)

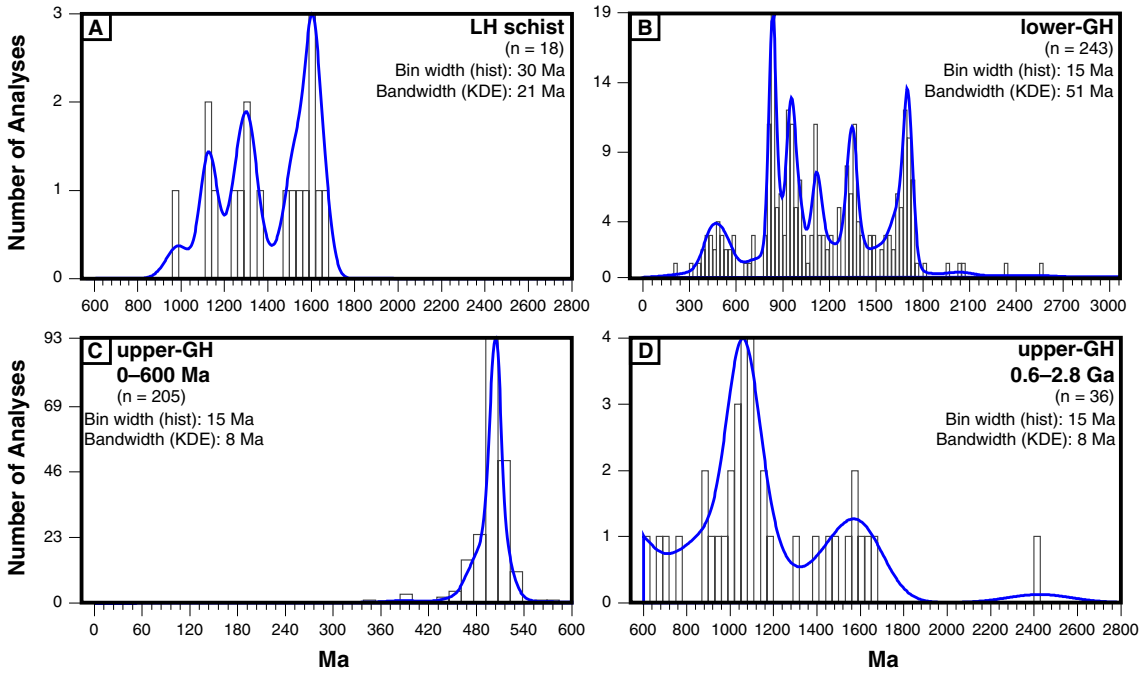

Fig. 2 Kernel density estimate plots for the pre-Himalayan (pre-Oligocene) zircons from the **a** LH sample; **b** lower-GH rocks; **c** the upper-GH, with dates from 0–600 Ma; and **d** the upper-GH, with >00 Ma dates. The upper-GH was divided into two separate plots due to the numerous ca. 500 Ma zircons. The bandwidth for each plot was calculated by DensityPlotter 3.1 (Vermeesh 2012) and represents the optimal value to prevent over/under smoothing

an *Agilent 7700x* quadrupole ICPMS, and a *Photon Machines Analyte* 193 laser-ablation system. For all zircon and monazite analyses, the ICPMS was operated in split-stream mode, in which the ablated material was split and analyzed by the MC-ICPMS for the U–Th–Pb ratios, and the SC-ICPMS (Attom or 7700x) for the trace-element abundances (see summary of technique in Kylander-Clark et al. 2013). The laser fluence was ~3–4 J/cm^2 for all analyses, producing an ablation rate of 0.05–0.10 μm/pulse and a typical pit depth of ~7 μm. The spot size was 20–30 μm depending upon the size of the zircon. For further details of the analyses, see the online supplementary material.

The U–Th–Pb isotopic zircon results are presented in kernel density plots (Fig. 2; DensityPlotter 3.1; Vermeesh 2012) for dates older than the Oligocene (or likely inherited dates) and in standard concordia diagrams for the Himalayan-age zircons (Figs. 3, 4, 5; Isoplot 3.75, Ludwig 2010). Results are also described in Table 1 and in online resource Table 1. Moreover, because monazite favors the incorporation of Th over U during crystallization, and because of the typical excess ^{206}Pb in monazite (Schärer 1984), ^{208}Pb/^{232}Th dates are reported for the monazite crystallization. The U–Th–Pb data are represented in ^{206}Pb/^{238}U versus ^{208}Pb/^{232}Th concordia plots (Fig. 8; U–Pb_Redux 2.50, Bowring et al. 2011; McLean et al. 2011), Table 1, and in online resource Table 2. All errors for both zircon and monazite results are reported at the two-sigma level. Uncertainties associated with all the geochronometric dates are a combination of analytical and propagated uncertainty, which accounts for the long-term standard reproducibility of ~2 % for the standards run during all sessions on the instruments.

Trace-element abundances were collected simultaneously with the U–Th–Pb isotopic measurements on either a *Nu Attom* single-collector ICPMS or an *Agilent* quadrupole ICPMS as described above. The rare-earth element (REE) patterns provide qualitative information about the likely presence or absence of minerals during zircon and monazite growth and therefore about the P–T conditions under which those phases crystallized. For example, if zircon growth occurred concurrently with garnet, zircon would exhibit depletion of the HREE due to the preferential incorporation of these elements into garnet (e.g., Rubatto and Hermann 2007). Nearly all of the zircons from both the lower-GH and the upper-GH in central and eastern Bhutan exhibit a negative Eu anomaly and a positive, moderate-to-steep heavy rare-earth element (HREE) pattern (Fig. 6; online resource Fig. 1).

In addition, for zircons analyzed with the *Agilent* quadrupole ICPMS, Ti concentrations were collected and used to determine Ti-in-zircon temperatures (Fig. 7, e.g., Watson et al. 2006; Ferry and Watson 2007; Fu et al. 2008). Ti-in-zircon temperatures were calculated using the

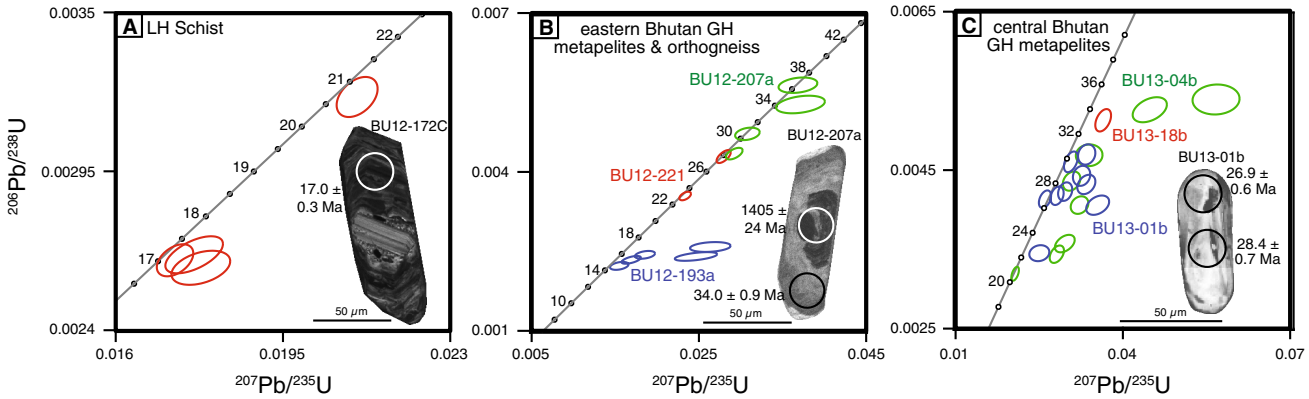

Fig. 3 Standard concordia plots of the Oligocene–Miocene zircon results from metasedimentary and orthogneiss samples from the **a** LH schist; **b** GH rocks from the eastern Bhutan transect; and **c** GH rocks from the central Bhutan transect. Each ellipse represents a single-spot analysis, and they are color-coded by sample number. Also shown are representative CL images with the 207-corrected age and spot labeled

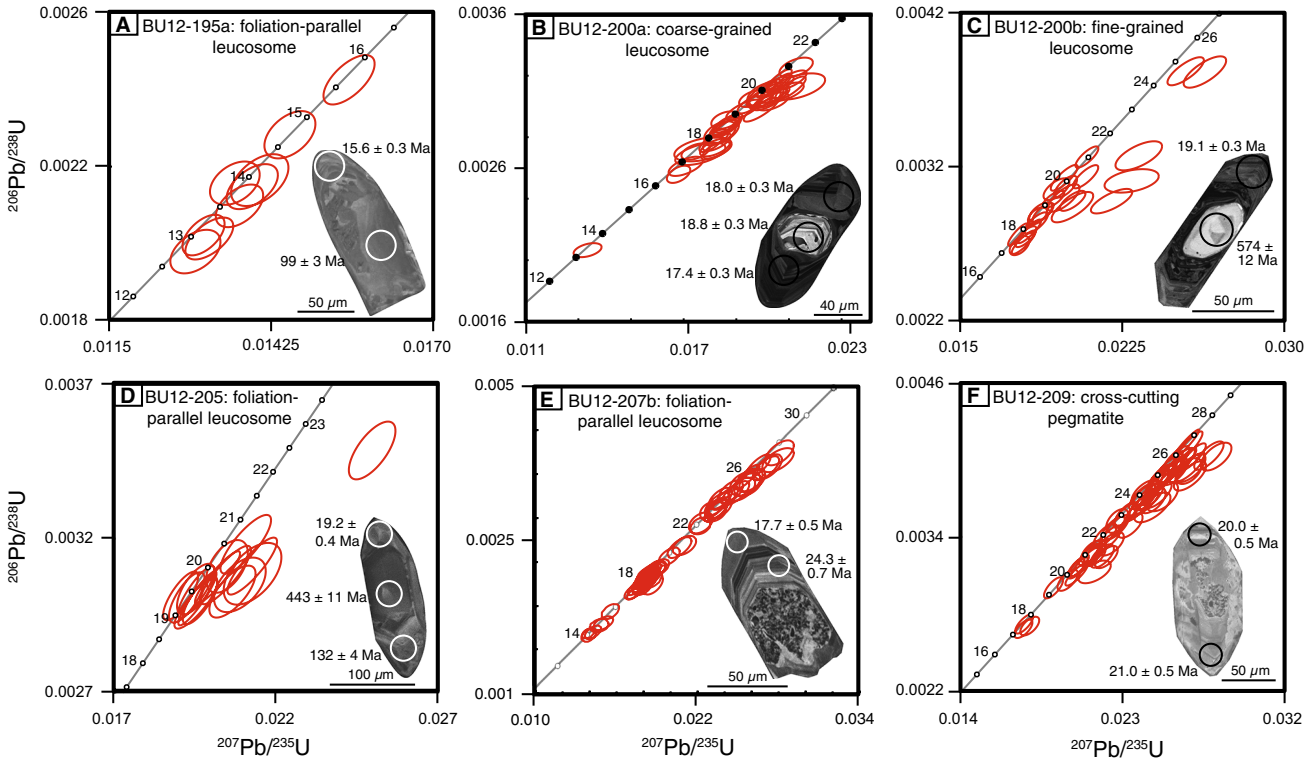

Fig. 4 Standard concordia plots of the Oligocene–Miocene zircon results from the leucosome samples from the eastern Bhutan transect, including: **a** BU12-195a, **b** BU12-200a, **c** BU12-200b, **d** BU12-205, **e** BU12-207a, and **f** BU12-209. Also shown are representative CL images with the 207-corrected age and spot labeled

calibration of Watson et al. (2006). For the temperature estimates, unit activities of TiO_2 and SiO_2 were assumed, and no pressure correction was applied. All samples contained quartz and the majority of samples contained ilmenite, with one sample containing rutile (Table 1). Two samples did not contain any Ti-bearing phase. For those samples that do not contain rutile, the temperatures are treated as minimum estimates.

Like zircon, monazite trace-element patterns give qualitative information about the conditions of crystallization. Because garnet and monazite both preferentially incorporate Y + HREE into their structures, trace-element patterns can reflect garnet presence or absence during monazite growth (e.g., Kohn et al. 2005). Details describing the monazite results from individual samples are reported below, as well as in online resource Table 4.

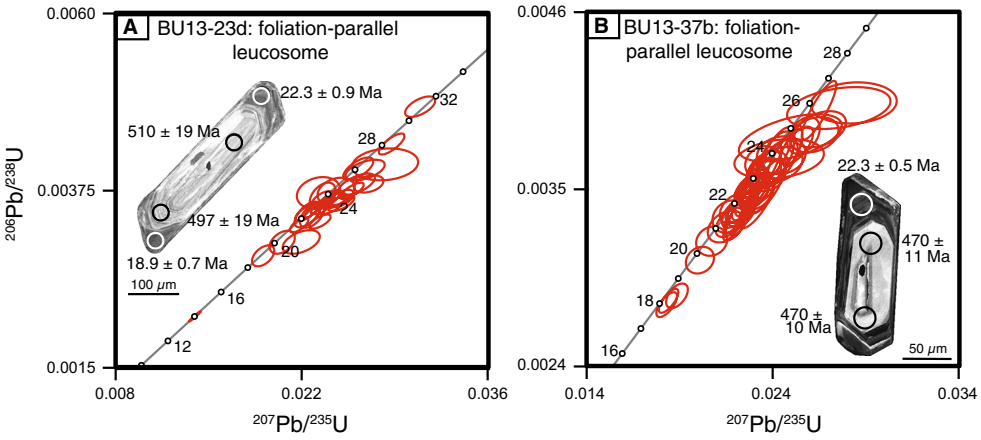

Fig. 5 Standard concordia plots of the Oligocene–Miocene zircon results from the leucosome samples from the central Bhutan transect, including: **a** BU13-23d and **b** BU13-37b. Also shown are representative CL images with the 207-corrected age and spot labeled

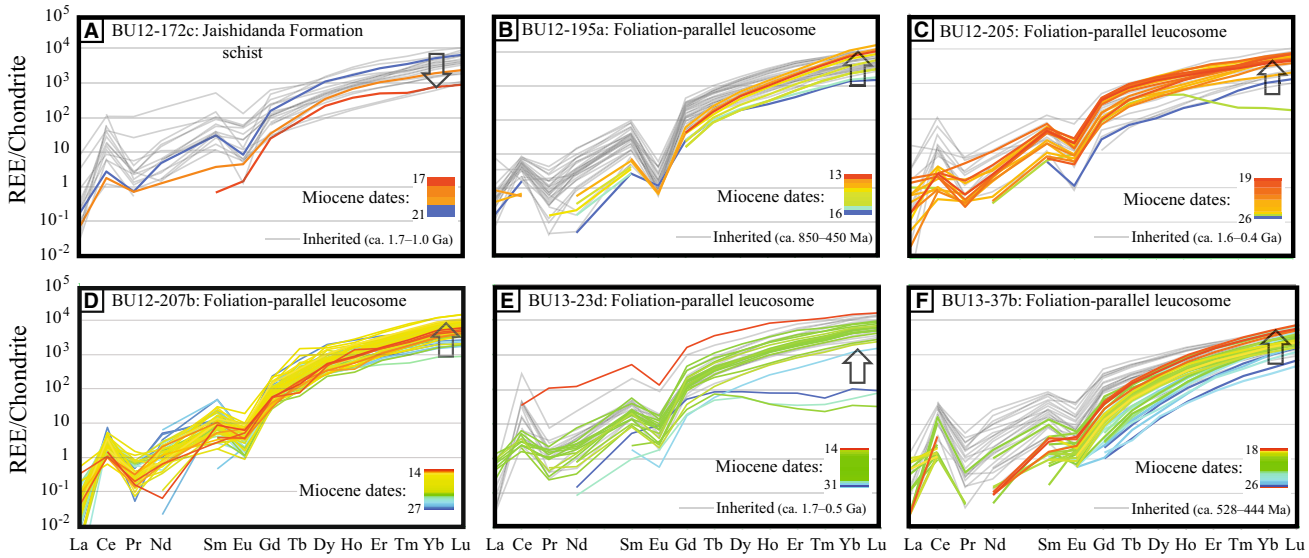

Fig. 6 Chondrite-normalized REE plots. Only samples that had a correlation between the age and composition are shown. The REE profiles are color-coded by date, and in addition, the *arrows* highlight the relevant change, with the *down arrow* indicating a decrease in the HREE over time, suggestive of garnet growth, and the *up arrow* indicating an increase in HREE over time and likely garnet breakdown. All REE values are normalized to the values of McDonough and Sun (1995). Samples include: **a** BU12-172, **b** BU12-195a, **c** BU12-205, **d** BU12-207b, **e** BU13-23d, and **f** BU13-37b

For the zircon data, only the age, trace element, and thermometry results from Himalayan-aged zircons are described in detail, with a brief discussion of the pre-Oligocene dates from all of the samples. Details on all of the studied samples are described in the online resource material.

Results

Pre-Oligocene zircon results

Within the LH, a schist from the Jashidanda Formation (BU12-172c), exposed directly below the MCT, was collected. The schist zircons mainly yielded inherited ages, with peaks at ca. 1.1, 1.3, and 1.6 Ga (Fig. 2). In comparison, the inherited zircons from the GH rocks revealed similar Proterozoic zircon age populations to the LH schist. However, these rocks also show younger age peaks, with the lower-GH rocks yielding peaks at ca. 0.5, 0.8, and 0.9 Ga (Fig. 2). In comparison, the upper-GH rocks are dominated by leucocratic samples, and they showed a prominent ca. 500 Ma peak, with smaller Proterozoic peaks at ca. 1.1 and 1.6 Ga.

Metamorphic and melt crystallization zircon results

As described above, most of the zircons from the metapelite and orthogneiss samples yielded inherited ages (online

resource material eTable 1), with minimal Himalayan growth on the rims of the zircons. For example, metasedimentary samples, BU12-178c, BU12-182, BU12-190b, and leucosome sample, BU12-190a, revealed only inherited ages. Therefore, the Himalayan U–Pb results from the metapelite and orthogneiss samples that did yield Oligocene–Miocene dates are grouped together in a single concordia diagram for each transect, in addition to a concordia diagram for the LH schist (Fig. 3). In comparison, the leucocratic samples yielded abundant Himalayan-aged zircons, and the data show a continuum of dates that are within error (Figs. 4, 5). However, there is a sufficient spread in time that a weighted mean age typically cannot be calculated from the dates within a single sample. Table 1 reports the range in the 207-corrected $^{206}Pb/^{238}U$ dates from each sample, and the Himalayan results from each leucosome and pegmatite are shown in individual concordia diagrams for each transect (Figs. 4, 5).

Metasedimentary rocks and orthogneisses

From the LH schist (BU12-172c), four zircon rims revealed dates ranging from ca. 21 to 17 Ma (Fig. 3a). Among these grains, there is a decrease in the abundance of HREE with decreasing age (Fig. 6a).

The eastern Bhutan GH transect revealed a range of zircon rim dates from two metapelites and an orthogneiss. The youngest dates were obtained from a metapelite collected within the KT zone (BU12-193a), and the zircons ranged from ca. 16 to 14.5 Ma (Fig. 3b). These grains also yielded Ti-in-zircon minimum temperatures of ~565–680 °C (Fig. 7). The oldest dates from this transect were obtained from a metapelite in the upper-GH (BU12-207b), with four zircon rims yielding dates of ca. 37 to 28 Ma (Fig. 3b). Finally, the structurally highest sample, orthogneiss BU12-221, revealed two dates of ca. 28 and 23 Ma (Fig. 3b).

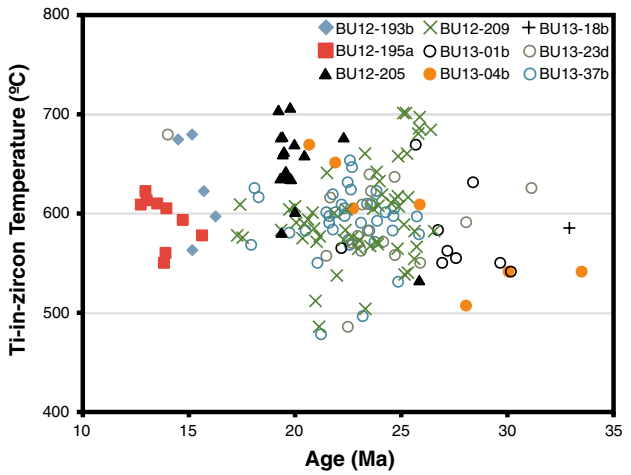

Fig. 7 Ti-in-zircon temperatures versus age for all zircons analyzed by the quadrupole ICPMS. All temperatures were calculated, assuming a Ti activity of 1; therefore, temperatures should be interpreted as a minimum. Note the relatively high temperatures (>550 °C) for the youngest Miocene dates of ca. 14–13 Ma

The samples (BU13-01b, 04b, 18b) from the central Bhutan GH transect were all collected within the lower-GH; however, they did not show dates as young as those observed in the lower-GH eastern Bhutan metapelite. The samples instead revealed a range of dates from ca. 33 to 20 Ma (Fig. 3c), and these grains yielded Ti-in-zircon minimum temperatures of ~510 to 670 °C (Fig. 7). None of the GH samples showed a correlation among dates and REE composition (online resource Fig. 1).

Leucosomes, Kuru Chu transect, eastern Bhutan

The upper-GH leucosomes showed only Himalayan-aged zircons. The foliation-parallel leucosome (BU12-195a) from just above the KT yielded some of the youngest dates (ca. 16 to 13 Ma) of the leucosomes (Fig. 4a). The Ti-in-zircon minimum temperatures ranged from ~550 to 620 °C (Fig. 7), and these grains showed an overall increase in the steepness of the HREE (Lu_n/Dy_n changes from 8 to 24) with decreasing age (Fig. 6b).

In comparison, the leucosomes from structurally higher levels within the upper-GH revealed progressively older age populations with increasing structural distance above the KT. Two foliation-parallel leucosomes, one coarse-grained (BU12-200a) and the other finer-grained (BU12-200b), were collected from the same outcrop. Both yielded abundant zircons from ca. 21 to 17 Ma (Fig. 4b, c). The coarser-grained leucosome also contained a young, ca. 13 Ma zircon (Fig. 4b), whereas the finer-grained leucosome contained a single zircon that yielded Oligocene, ca. 25 Ma, core dates (Fig. 4c).

Foliation-parallel leucosome (BU12-205) also yielded similar results to these two leucosomes, with a population of ca. 20 Ma zircons, with a single outlier grain at ca. 26 Ma (Fig. 4d). Ti-in-zircon temperatures from these zircons revealed that minimum temperatures ranging from ~530 to 710 °C that for the most part did not correlate with age; however, the oldest, ca. 26 Ma, zircon did yield the lowest temperature of 530 °C (Fig. 7). Moreover, the oldest, ca. 26 and 22 Ma, grains show a distinct flatter HREE pattern in comparison with the other Himalayan grains (Fig. 6c).

The next two structurally higher leucosomes revealed a much wider spread in zircon crystallization (>10 Myr) and revealed some of the oldest leucosome crystallization dates. Zircons with relatively simple zoning from a foliation-parallel leucosome (BU12-207b) gave dates of ca. 27–22 Ma, whereas some grains also exhibited an additional unzoned, outermost rim (Fig. 4e). These unzoned rims yielded the

younger age populations at ca. 18 and 14 Ma (Fig. 4e). The chemistry of these zircons overall revealed a general age trend in which the steepness of the HREE increased (from Lu_n/Dy_n of 2.4 to 12) as the dates became younger (Fig. 6d). Structurally above this, a crosscutting pegmatite (BU12-209) yielded a similar continuum of dates from ca. 27 to 19 Ma, with a younger population of grains at ca. 17 Ma (Fig. 4f). The Ti-in-zircon thermometry showed a range of minimum temperature results from the pegmatite, from ~510 to 700 °C; temperatures did not correlate with age (Fig. 7).

Leucosomes, Bumthang Chu transect, central Bhutan

Leucosome samples were only analyzed from the upper-GH on the central Bhutan transect due to poor exposure and the large volume of quartzite and marble in the lower-GH in this transect. The two foliation-parallel leucosome samples revealed similar zircon crystallization ages to the structurally higher samples in the eastern Bhutan transect, with most of the zircons crystallizing from ca. 27 to 20 Ma (Fig. 5).

Zircons extracted from a folded leucosome (BU13-23d) showed two types of zircons. Some zircons had oscillatory-zoned cores and unzoned rims, whereas others had oscillatory-zoned or unzoned cores mantled by a darker, oscillatory zone, in addition to an outermost unzoned rim. Unzoned rims from this first type of zircon yielded dates ranging from ca. 28 to 24 Ma (Fig. 5a). From the second type of zircon, the mantle zircon zone had dates of ca. 24–22 Ma and the outermost, unzoned rims gave the youngest dates of ca. 22–19 Ma, with a single isolated grain at ca. 14 Ma (Fig. 5a). Of these zircons, only the 14 Ma grain yielded a distinct REE pattern: Overall, it had the highest REE abundances, and it yielded a relatively flat HREE profile ($Lu_n/Dy_n = 3.1$; Fig. 6e). Moreover, the zircons showed a Ti-in-zircon minimum temperature range of ~500–680 °C with no major age trend (Fig. 7).

Zircons from the other pegmatitic leucosome (BU13-37b) yielded a range of dates: ca. 26–20 Ma, with a younger population of three analyses at ca. 18 Ma (Fig. 5b). These Himalayan-age grains all revealed similar steep HREE patterns; however, the general REE abundances increased and the overall steepness of the HREE pattern decreased with decreasing age (e.g., a ca. 26 Ma grain had a $Lu_n/Dy_n = 49$ versus the ca. 18 Ma grain revealed a $Lu_n/Dy_n = 17$) (Fig. 6f). Ti-in-zircon minimum temperature results ranged from ~500 to 650 °C for the Oligocene–Miocene zircons and did not correlate with age (Fig. 7).

Monazite geochronology

As there were not many Himalayan-aged zircons obtained from the lower-GH, monazite was extracted and analyzed from four of the lower-GH eastern Bhutan samples. Overall, the monazite dates clustered around ca. 15 Ma (Fig. 8), and the grains from all samples had a strong negative Eu anomaly and a steep negative HREE slope, with Yb/Gd ratios ranging from 0.01 to 0.05 (Fig. 9). While there is some variation in the abundance of Y and the slope of the HREE pattern within individual samples, the patterns in the majority of the samples do not correlate with age (Fig. 8).

A single monazite grain was separated from schist sample BU12-178c. Three spot analyses near the rim of the crystal and one near the crystal core yielded a weighed-mean average age of 15.0 ± 0.5 Ma (MSWD = 0.7; Fig. 8a). Despite the lack of difference in the age, these core and rim spots contained differences in their Y chemistry, with higher values in the two rims (1.0 and 1.6 wt%) in comparison with the core analyses (~0.6 wt%; Fig. 8a). In comparison, Th concentrations were consistent (4.0–4.9 wt%) throughout the grain.

Slightly older dates were obtained from metapelite BU12-182, with monazite dates ranging from ca. 17 to 15 Ma (Fig. 8b). Moreover, an additional monazite yielded a ca. 31 Ma Oligocene date. Overall, there was significant variability in the chemistry among grains, with Y and Th varying from 0.7 to 1.3 and 4.3 to 7.0 wt%, respectively. Four additional monazites yielded pre-Himalayan dates, ranging from ca. 110 to 680 Ma.

From the foliation-parallel leucosome, BU12-190a, and the metapelite, BU12-193a, monazites yielded little variation in dates among and within grains, with dates of ca. 14 to 15 Ma (Fig. 8c, d). Among the leucosome grains, there was some variability in the Y content, with values ranging from 0.6 to 1.7 wt% (Fig. 8c). In comparison, the HREE patterns from the metapelite grains showed two distinct populations that did not correlate with age (Fig. 9c). In addition, the Y and Th concentrations were variable among the grains, ranging from 0.3 to 1.8 and 3.8 to 6.7 wt%, respectively. For the metapelite, the Y does correlate with age, with the younger ca. 14 Ma monazites having a higher Y content (Fig. 8d).

Discussion

Age constraints on GH sedimentary and igneous protoliths

Most of the pelitic samples from the lower- and upper-GH in central and eastern Bhutan revealed a range of detrital ages between ca. 1800 and 800 Ma (Fig. 2). In addition, several samples also contained dates as young as ca. 500 Ma. Previous detrital zircon studies of the GH in other parts of the Himalaya have revealed similar detrital-age patterns and have argued that the ca. 1800–1600 Ma

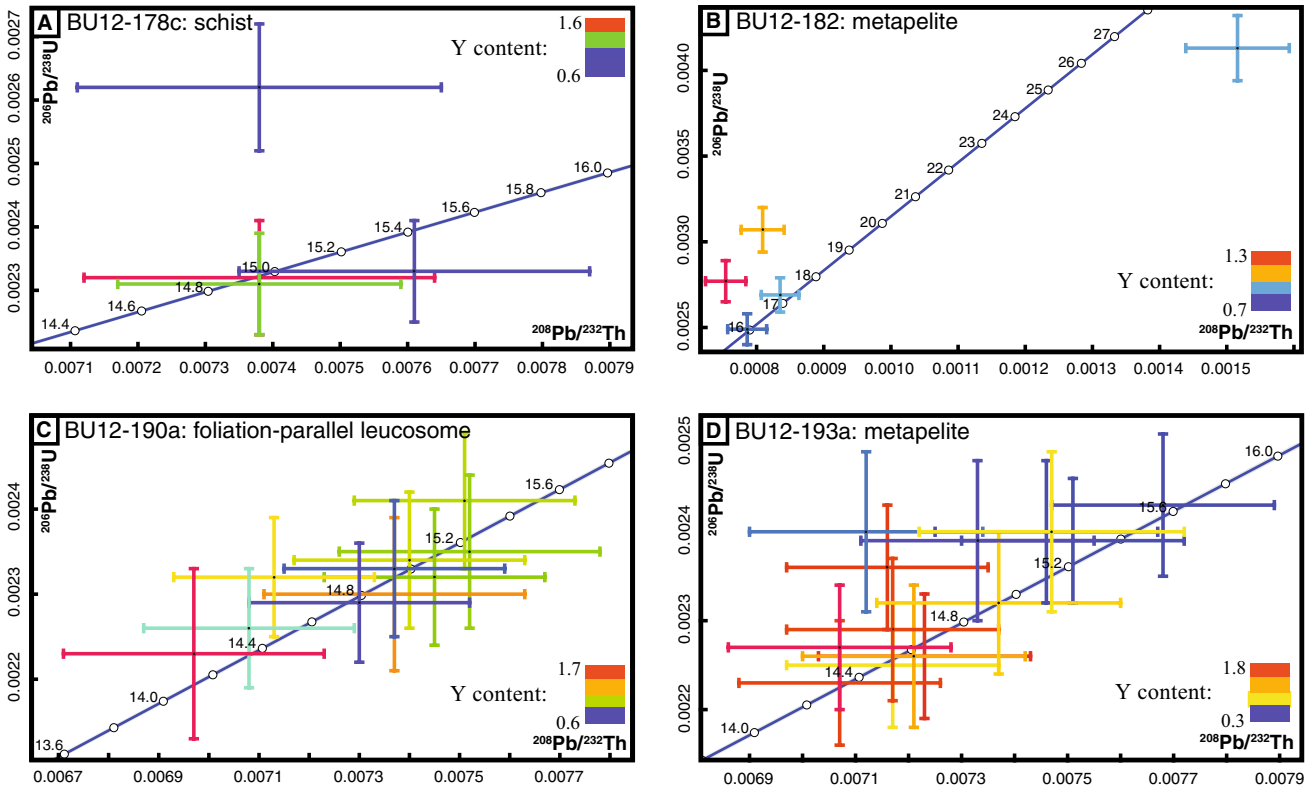

Fig. 8 $^{206}Pb/^{238}U$ versus $^{208}Pb/^{232}Th$ concordia plots showing the monazite results for samples: **a** BU12-178c, **b** BU12-182, **c** BU12-190a, and **d** BU12-193a. Each *cross* represents a single-spot analysis; they are color-coded by the corresponding Y content, and the *color bar* shows the representative gradient in colors and how they correspond to Y concentrations (shown in wt%)

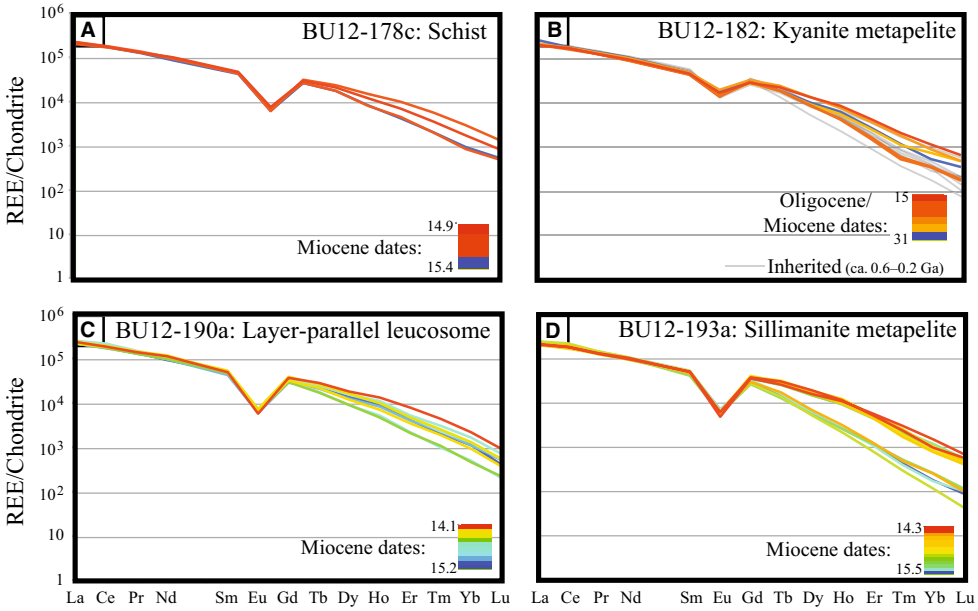

Fig. 9 Chondrite-normalized rare-earth element (REE) plots, showing the REE composition of the dated monazite. All REE values are normalized to the values of McDonough and Sun (1995). Samples include: **a** BU12-178c, **b** BU12-182, **c** BU12-190a, and **d** BU12-193a

detrital zircon populations were sourced from Paleoproterozoic orogenic events along the Indian shield (Parrish and Hodges 1996; Kohn et al. 2010; Long et al. 2011a; McQuarrie et al. 2013), whereas the younger detrital ages have been interpreted to represent detritus associated with late Neoproterozoic to Cambrian orogenesis that occurred

along the eastern margin of India (Myrow et al. 2010; McQuarrie et al. 2013). Finally, the Late Cambrian–Ordovician dates are similar to other dated orthogneiss bodies within the GH in Bhutan (Long and McQuarrie 2010; Long et al. 2011c) and across the orogen (Gehrels et al. 2003; Cawood and Buchan 2007). These orthogneisses have been interpreted to represent granitic intrusions that were likely accompanied by metamorphism during the Bhimphedian orogeny, a Cambrian–Ordovician event that affected the northern Indian margin (e.g., Cawood and Buchan 2007). Protoliths for other well-documented Himalayan granitic intrusions have been dated at ca. 2600 Ma, ca. 830 Ma, and ca. 750 Ma (e.g., Miller et al. 2001).

Eocene–Miocene metamorphism and melt crystallization

The Eocene–Miocene U–Th–Pb dates from zircon and monazite extracted from these metasedimentary rocks and related granitic intrusions are interpreted to record syn-Himalayan metamorphism, melt crystallization, and the initiation of GH exhumation. The zircon and monazite data are presented in a compilation diagram comparing the dates from each sample versus structural position (Fig. 10) and are summarized below.

Metamorphism

Eocene–Miocene dates, ca. 36–24 Ma in eastern Bhutan and ca. 33–21 Ma in central Bhutan, were revealed in the metapelite and orthogneiss zircons (Figs. 3, 10), likely recording prograde-to-peak metamorphism. Other Himalayan studies have described similar dates (ca. 35–32 Ma in the central Himalaya and ca. 35–25 Ma in the western Himalaya) from metasedimentary GH samples and have interpreted them to record prograde metamorphism associated with underthrusting of the GH protoliths beneath a fold–thrust belt that developed in Tethyan Himalayan rocks that formed during the early, post-collisional phases of India–Asia convergence (Vannay and Hodges 1996; Hodges et al. 1996; Yin and Harrison 2000; Godin et al. 2001; Leech et al. 2005; Corrie and Kohn 2011).

Zircons from one metapelite (BU12-193a) and monazite dates from the same metapelite and from a schist (BU12-178c) and an additional metapelite (BU12-182), all from the lower-GH in eastern Bhutan, suggest that metamorphism continued until ca. 14 Ma. This is consistent with the timing of metamorphism documented in upper-GH rocks to the west [e.g., western Bhutan (Grujic et al. 2011; Warren et al. 2011b); Ama Drime Massif (Cottle et al. 2009; Rubatto et al. 2013)] and to the east (e.g., Arunachal Pradesh (Warren et al. 2014).

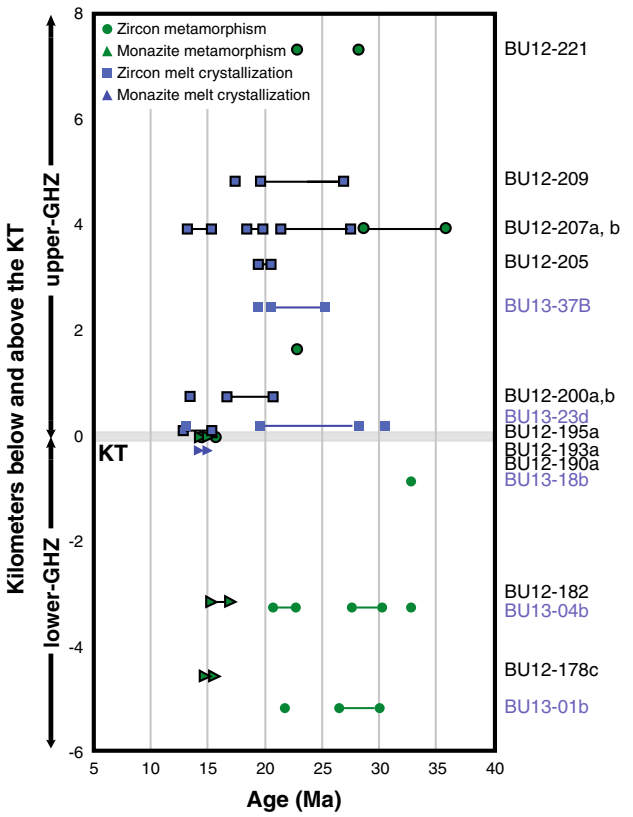

Fig. 10 Summary of 207-corrected $^{206}Pb/^{238}U$ zircon and $^{208}Pb/^{232}Th$ monazite dates for the individual samples analyzed across the two transects. The samples and dates are shown relative to their structural distance from the KT. The zircon (*circles*) and monazite (*triangles*) dates are categorized as recording metamorphism (*green*) or melt crystallization (*blue*). The *lines connecting symbols* indicate where there is a continuous spread of zircon dates. Samples from the eastern Bhutan transect have a *black outline around the symbols* and have *black text* for the sample label, whereas samples from the central Bhutan transect lack a *black outline*, and the sample label is shown in *blue*

Melt crystallization

The majority of the studied samples that yielded Himalayan-aged zircons were the leucosomes, and the results from both the central and the eastern Bhutan transects suggest protracted melt crystallization during the Oligocene to Miocene. From the eastern Bhutan transect, the majority of the leucosomes showed crystallization from ca. 20 to 18 Ma, with some older crystallization (up to ca. 27 Ma) in the two structural highest studied leucosomes (BU12-207b and BU12-209). Samples, BU12-200b and BU12-205, are examples of leucosomes that yielded the dominant ca. 20–18 Ma zircon populations, but they also contained zircons that revealed older, isolated Oligocene dates (Fig. 4c, d); however, these dates were considered outliers and not interpreted in terms of melt crystallization, which should

have resulted in abundant zircon growth (e.g., Kelsey et al. 2008).

Several leucosome samples also document continued melt crystallization as young as ca. 14–13 Ma (BU12-195a, BU12-200a, BU12-207b) from all structural levels of the upper-GH. While sample BU12-190a did not yield any Miocene zircons, monazite from this leucosome likely dates melt crystallization in the lower-GH rocks at ca. 15–14 Ma. Overall, the data from the leucosomes in eastern Bhutan do not reveal any change in the timing of the youngest melt crystallization across the KT.

The two leucosomes from the central Bhutan transect suggest the same protracted crystallization history, from ca. 25 to 18 Ma, observed in the structurally higher samples from the eastern Bhutan transect. Leucosome, BU13-23d, did also yield a single, concordant, ca. 14 Ma zircon.

Besides the Oligocene to Miocene zircons, multiple leucocratic samples revealed ca. 500 and 830 Ma zircon populations (BU12-195a, BU13-23d, 37b), and these samples provide evidence that there were multiple generations of melt present within the two studied transects. Zircon commonly forms during melting (e.g., Hermann and Rubatto 2003; Kelsey et al. 2008); therefore, the absence of or lack of abundant Himalayan zircons within multiple of the studied leucosomes, combined with the abundance of ca. 500 Ma zircons, argues that some of the observed migmatization likely occurred during the Cambrian (e.g., related to the Bhimphedian orogeny). Thus, these results suggest that there are probably a mix of both Oligocene/Miocene and Cambrian leucosomes found throughout central and eastern Bhutan.

Rock assemblages and trace-element analyses: linking dates to the P–T path

Overall, the metapelite mineral assemblage, with a change from kyanite as the dominant aluminosilicate to sillimanite, and an overall increasing percentage of leucocratic material with increasing structural distance above the MCT suggest that higher-temperature conditions were achieved from the rocks with increasing structural distance above the MCT. Swapp and Hollister (1991) argued, based on mineral assemblages, that upper-GH rocks had crossed the second sillimanite isograd, and they further argued that the GH rocks underwent a near-isothermal decompression path, due to the presence of cordierite. The majority of their samples were from western Bhutan, where these qualitative observations have been supported through later thermobarometry work (Grujic et al. 2011; Warren et al. 2011a, b). However, in central and eastern Bhutan, there is no evidence that the rocks have crossed the second sillimanite isograd. There is abundant muscovite found in the metasedimentary rocks, although the overall percentage of muscovite does decrease and K-feldspar is found in some of the metapelites near sample BU12-209. Moreover, cordierite has not been observed in any of the collected samples.

Based on these observations and the lack of any quantitative thermobarometric data from central and eastern Bhutan, simplified P–T paths have been made for different structural levels of the GH (Fig. 11); here, we focus on eastern Bhutan given the larger number of studied samples from this transect. The constraints for the P–T paths, plotted on a simplified KFMASH compositional diagram, consist of: (1) for the lower-GH (based on samples BU12-178 BU12-182), the presence of kyanite and muscovite but no cordierite; (2) for rocks in the structurally lower part of the upper-GH (samples BU12-190a,b, BU12-193, BU12-195, BU12-200a,b, BU12-205), the presence of sillimanite, muscovite, and no cordierite; and (3) for rocks in the structurally higher part of the upper-GH (samples BU12-207, BU12-209), sillimanite, smaller amounts of muscovite (possible crossing of the second sillimanite isograd), and no cordierite.

Timing constraints can be placed on these P–T paths using the zircon and monazite results that revealed the timing of metamorphism and melt crystallization, assuming that the rocks had to have surpassed their peak P–T conditions by the time that melt crystallization initiated. Therefore, the lower-GH rocks underwent peak metamorphism >15 Ma (based on the monazite melt crystallization dates from BU12-190a). In comparison, the upper-GH rocks record a much different history, with peak metamorphism occurring >21 Ma in the structurally lower levels of the upper-GH and >27 Ma in the structurally higher levels of the upper-GH (Fig. 11). Therefore, based on the melt crystallization results, there is a trend with structural distance above the MCT in the eastern Bhutan GH rocks, with cooling and probable initial exhumation beginning earlier with increasing structural distance above the MCT. The two leucosome samples from central Bhutan also suggest an early cooling history, with melt crystallization occurring by ca. 25 Ma.

These cooling and probable exhumation results are also supported by the zircon trace-element data. This study focuses mainly on the availability of the HREE, which commonly are incorporated into accessory phases, such as zircon, monazite, xenotime, and garnet (Rubatto 2002). There are age trends in the zircon trace-element data within six of the samples that describe when more or less HREEs were available for the zircon to take in during crystal growth. The results can therefore describe when the breakdown of garnet occurs, which is likely associated with the initial stages of decompression (e.g., Spear et al. 1999; Rubatto et al. 2013). In the central Bhutan leucosome samples, the oldest Oligocene dates revealed the lowest Lu_n/

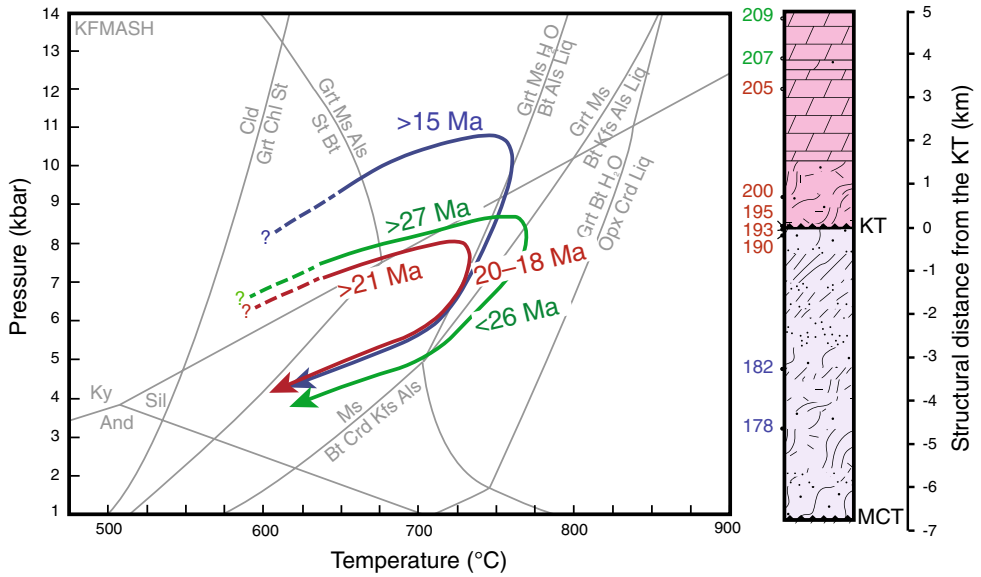

Fig. 11 Representative P–T paths from different structural locations within the GH. The shape of the paths was determined by the mineral assemblage of the rocks and is plotted on a KFMASH petrogenetic grid with select reactions from Wei et al. (2004). The timing constraints are based on the zircon and monazite metamorphic (dating the prograde-to-peak portion of the path) and melt crystallization (dating the time at which the rocks had to have begun the retrograde portion of the path) results from the samples shown in the tectonostratigraphic column to the right of the P–T path. *Blue* the structurally lowest GH samples; *Red* the middle of the package of GH rocks; and *Green* the structurally highest GH samples

Dy_n ratios. In particular, the oldest (ca. 31–25 Ma) dates from BU13-23d showed a flat HREE profile that were distinct from the other Oligocene–Miocene (ca. 24–14 Ma) dates from the sample (Fig. 7e). In both leucosomes, these age trends suggested that more HREEs were available within the system post-25 Ma, reflecting that garnet breakdown occurred post-25 Ma. Several of the foliation-parallel leucosomes from eastern Bhutan (BU12-195a, 207b) show similar trends, where the older Oligocene dates revealed the lowest Lu_n/Dy_n ratios, and the HREE ratios increased with decreasing age. Interestingly, the one LH sample analyzed from below the MCT, the Jaishidanda Formation schist (BU12-172), showed the opposite trend compared to the GH samples: The HREE patterns became more flat from ca. 21 to 17 Ma (Fig. 6a), suggesting garnet growth over this time interval and therefore that these dates are likely recording prograde-to-peak metamorphism.

Despite the zircon results that in some cases document relatively early (ca. 27 Ma) cooling to induce melt crystallization, multiple samples from the lower- and upper-GH record continued melt crystallization and metamorphism until ca. 14–13 Ma (Fig. 10). The Ti-in-zircon temperatures from these Miocene zircons reveal >550 °C crystallization temperatures (Fig. 7), suggesting that cooling and initial exhumation may have occurred to cause melt crystallization and garnet breakdown, but the rocks were not exhumed to shallow crustal conditions until post-13 Ma.

Himalayan structures in eastern and central Bhutan

Differences in the conditions and timing of metamorphism and melt crystallization within Himalayan rocks have been a principal technique used to identify major structures (e.g., Martin et al. 2011; Warren et al. 2011b; Rubatto et al. 2013; Warren et al. 2014). Comparing the youngest metamorphic and/or melt crystallization dates from all of the GH metasedimentary and leucocratic rocks shows very similar results of ca. 14–13 Ma across the previously mapped KT (Swapp and Hollister 1991; Grujic et al. 2002). The new data thus do not show a difference in the youngest melt crystallization and metamorphic ages from the lower-GH in comparison with the upper-GH. Studies in northwestern Bhutan, however, have recorded distinct age differences across the Laya thrust (Kellett et al. 2009, 2010; Warren et al. 2011b; Grujic et al. 2011). There, monazite metamorphic ages vary from ca. 21–17 Ma within the lower-GH to ca. 15–14 Ma within the upper-GH, and melt crystallization ages also decrease across the Laya thrust, from ca. 23–15 Ma within the lower-GH (zircon and monazite; Carosi et al. 2006; Kellett et al. 2010) to ca. 15–11 Ma in the upper-GH (zircon and monazite; Kellett et al. 2009; Warren et al. 2011b). The differences in the timing of melt crystallization and metamorphism across the Laya thrust in comparison with the KT suggest that the two structures likely do not connect along strike, as initially interpreted by

Grujic et al. (2011) and Long et al. (2011c). Furthermore, given the lack of evidence for differences in the metamorphic dates throughout the GH section, nor any evidence for a crossing of the second sillimanite isograd (which was originally how the structure was mapped (Swapp and Hollister 1991), the KT may represent a minor, second-order shear zone rather than a major Himalayan structure.

Cooling and exhumation of GH rocks

Multiple models have been proposed for driving the emplacement of the GH, with the critical taper-type (e.g., Davis et al. 1983) and channel flow-type (e.g., Beaumont et al. 2001) exhumation models representing end members. Each of these end-member models makes specific predictions about the timing of melt crystallization and metamorphism with structural distance through the GH. Critical-taper end-member models predict that melt crystallization and metamorphism would occur homogeneously across the GH, with a younging in those ages close to the lower-bounding structure (Kohn 2008). In comparison, in the channel-flow end-member models, the center of the channel has been translated farther than the channel edges and remains hotter longer, resulting in the youngest melt crystallization and metamorphic ages in the center of the channel (Beaumont et al. 2001; Jamieson et al. 2004).

The upper-GH in central and eastern Bhutan had been interpreted as a channel bound by the KT and inner STD, and it was thought to have been emplaced from ca. 15–11 Ma during synchronous activity on these bounding structures (Grujic et al. 2002; Hollister and Grujic 2006). However, as described above, the new zircon and monazite geochronology data presented in this study indicate that the youngest melt crystallization ages were consistently ca. 14–13 Ma (Fig. 10) and that the KT is likely a minor intra-GH shear zone. If the KT is not a major structure, the data from the entire GH can be examined as a whole. In this scenario, emplacement and initial exhumation would have occurred during motion on the MCT (ca. 23–13 Ma; Grujic et al. 2002; Daniel et al. 2003; Kellett et al. 2009, 2010; Chambers et al. 2011).

The overall decrease in the initiation of melt crystallization dates with lower structural position within the GH unit presented here is consistent with initial emplacement and cooling of the GH through progressive underplating of material likely along minor shear zones, given the lack of evidence for major thrust structures throughout the GH unit. The cooling may have been driven either through motion on the outer STD or through surface erosion that accompanied the growth of the overall structural system. The underplating of ductile material and minor exhumation lasted until ca. 15 Ma (melt crystallization age of lower-GH sample BU12-190a), and the entire package of rocks must have remained at >550 °C until 14–13 Ma (youngest melt crystallization and metamorphic dates), prior to final exhumation. By ca. 11 Ma ($^{40}Ar/^{39}Ar$ muscovite cooling ages; Stüwe and Foster 2001; Kellett et al. 2009), GH rocks in western Bhutan were exhumed below the muscovite closure temperature (ca. 400 °C; Harrison et al. 2009). Thermochronology data are needed from central and eastern Bhutan to determine whether final cooling of the GH rocks occurred at a similar time to western Bhutan.

GH Rocks across the Himalayan orogen

The geochronology of the Himalaya exposed in regions surrounding Bhutan provides important context for the timing and processes driving metamorphism, melt crystallization, deformation, and exhumation in the eastern part of the orogen. Immediately west of the study area, the upper-GH above the Laya thrust in western Bhutan, and within the Ama Drime Massif to the west, reached eclogite-facies followed by granulite-facies conditions (Cottle et al. 2009; Grujic et al. 2011; Warren et al. 2011b). Melt crystallization and metamorphism in western Bhutan occurred over a short interval of time, with ca. 14 Ma granulite-facies metamorphism followed by melt crystallization at ca. 13 Ma (monazite; Grujic et al. 2011; Warren et al. 2011b). These dates are similar to the youngest metamorphic and melt crystallization dates recorded in the upper-GH in zircon from both the central and the eastern Bhutan transects of this study. The upper-GH rocks of western Bhutan do not record the protracted melt crystallization history observed in this study; however, lower-GH in western Bhutan has yielded a similar range of monazite and zircon melt crystallization ages (ca. 25–15 Ma) (Warren et al. 2011b; Carosi et al. 2006; Tobgay et al. 2012) in comparison with the lower-GH in central and eastern Bhutan.

East of Bhutan, in western Arunachal Pradesh, a diachronous metamorphic history has also been documented across the Zimithang thrust, a structure that has also been correlated with the KT (Yin et al. 2010b), with 17–13 Ma monazite dates obtained in the hanging-wall rocks and 27–17 Ma dates from footwall rocks. Several thermochronology analyses reveal $^{40}Ar/^{39}Ar$ muscovite dates of ca. 9–7 Ma within the same GH section both above and below the Zimithang thrust (Mathew et al. 2013; Warren et al. 2014). The new zircon and monazite geochronology from this study fills a gap in data for the eastern Himalaya and illustrates that while general timing relationships for metamorphism and melt crystallization are similar for GH rocks in all parts of Bhutan and in Arunachal Pradesh, central and eastern Bhutan do not show evidence for the major out-of-sequence thrusting documented in these other regions of the eastern Himalaya. Instead within eastern and central Bhutan, the GH needs to be treated as a single unit in regard to interpretations of emplacement models.

Conclusions

The integration of zircon and monazite geochronology and trace-element geochemistry over a large structural distance and across multiple structures, including the MCT and the KT, has provided new insight into the tectonic history of the GH in central and eastern Bhutan. The new data show that the GH remained at temperatures of >550 °C until ca. 14–13 Ma both structurally above and below the KT. The lack of an age trend across the GH suggests that the KT was not as significant of a structure as originally proposed (i.e., a channel-bounding structure; e.g., Grujic et al. 2002; Fig. 10). The data also revealed a downward younging in the initiation of melt crystallization through the GH, suggesting that initial emplacement of the GH occurred due to progressive underplating of ductile material.

Acknowledgments Field work in Bhutan was facilitated and made possible by the help of Ugyen Wangda (Chief Geologist/Head), Tashi Tenzin and Tobgay Tobgay of the Bhutan Department of Geology and Mines, as well as Sherub Wangdi of the Tourism Council of Bhutan. We thank Gareth Seward for his help with the SEM at UC Santa Barbara. This work was supported by the National Science Foundation grant EAR-1220300 to Gordon and Long.

References

Beaumont C, Jamieson RA, Nguyen MH, Lee B (2001) Himalayan tectonics explained by extrusion of a low-viscosity crustal channel coupled to focused surface denudation. Nature 414:738–742. doi:10.1038/414738a

Bhargava ON (1995) The Bhutan Himalaya: a geological account. Spec Publ Ser Geol Surv India 39:245

Bowring JF, McLean NM, Bowring SA (2011) Engineering cyber infrastructure for U–Pb geochronology: tripoli and U–Pb redux. Gochem Geophys Geosyst 12:Q0AA19. doi:10.1029/2010GC003479

Burbank DW, Beck RA, Mulder T (1996) The Himalayan foreland basin. In: Yin A, Harrison TM (eds) The tectonics of Asia. Cambridge University Press, New York, pp 205–226

Burchfiel BC, Zhiliang C, Hodges KV et al (1992) The south Tibetan detachment system, Himalayan orogen: extension contemporaneous with and parallel to shortening in a collisional mountain belt. Geol Soc Am Spec Publ 269:41

Carosi R, Montomoli C, Visonà D (2006) Normal-sense shear zones in the core of Higher Himalayan Crystallines (Bhutan Himalaya): evidence for extrusion? in channel flow, ductile extrusion and exhumation in continental collision zones, edited by RD Law, MP Searle, and L Godin. Geol Soc Am Spec Publ 268:425–444

Cawood PA, Buchan C (2007) Linking accretionary orogenesis with supercontinent assembly. Earth Sci Rev 82:217–256. doi:10.1016/j.earscirev.2007.03.003

Chakungal J, Dostal J, Grujic D et al (2010) Provenance of the Greater Himalaya sequence: evidence from mafic granulites and amphibolites in NW Bhutan. Tectonophysics 480:198–212. doi:10.1016/j.tecto.2009.10.014

Chambers J, Parrish R, Argles T et al (2011) A short-duration pulse of ductile normal shear on the outer South Tibetan detachment in Bhutan: alternating channel flow and critical taper mechanics of the eastern Himalaya. Tectonics 30:TC2005. doi:10.1029/2010TC002784

Corrie SL, Kohn MJ (2011) Metamorphic history of the central Himalaya, Annapurna region, Nepal, and implications for tectonic models. Geol Soc Am Bull 123:1863–1879. doi:10.1130/B30376.1

Corrie SL, Kohn MJ, Vervoort JD (2010) Young eclogite from the Greater Himalayan Sequence, Arun Valley, eastern Nepal: P–T–t path and tectonic implications. Earth Planet Sci Lett 289:406–416

Corrie SL, Kohn MJ, McQuarrie N, Long SP (2012) Flattening the Bhutan Himalaya. Earth Planet Sci Lett 349–350:67–74. doi:10.1016/j.epsl.2012.07.00

Cottle J, Searle M, Horstwood M, Waters D (2009) Timing of midcrustal metamorphism, melting, and deformation in the Mount Everest region of southern Tibet revealed by U(–Th)–Pb geochronology. J Geol 117:643–664. doi:10.1130/B25659.1

Daniel CG, Hollister LS, Parrish RR, Grujic D (2003) Exhumation of the Main Central Thrust from lower crustal depths, eastern Bhutan Himalaya. J Metamorph Geol 21:317–334. doi:10.1046/j.1525-1314.2003.00445.x

Davidson C, Grujic DE, Hollister LS et al (1997) Metamorphic reactions related to decompression and synkinematic intrusion of leucogranite, High Himalayan crystallines, Bhutan. J Metamorph Geol 15:593–612. doi:10.1029/JB088iB02p01153

Davis D, Suppe J, Dahlen FA (1983) Mechanics of fold-and-thrust belts and accretionary wedges. J Geophys Res 88:1153–1172

DeCelles PG, Gehrels GE, Quade J et al (1998) Neogene foreland deposits, erosional unroofing, and the kinematic history of the Himalayan fold–thrust belt, western Nepal. Geol Soc Am Bull 110:2–21

DeCelles PG, Robinson DM, Zandt G (2002) Implications of shortening in the Himalayan fold–thrust belt for uplift of the Tibetan Plateau. Tectonics 21:1062–1087. doi:10.1029/2001TC001322

DeCelles PG, Gehrels GE, Najman Y, Martin AJ, Carter A, Garzanti E (2004) Detrital geochronology and geochemistry of Cretaceous-Early Miocene strata of Nepal: implications for timing and diachroneity of initial Himalayan orogenesis. Earth Plan Sci Lett 227:313–330

Ding L, Kapp P, Wan XQ (2005) Paleocene-Eocene record of ophiolite obduction and initial India-Asia collision, south central Tibet. Tectonics 24:TC3001. doi:10.1029/2004TC001729

Edwards MA, Harrison TM (1997) When did the roof collapse? Late Miocene north-south extension in the high Himalaya revealed by Th-Pb monazite dating of the Khula Kangri granite. Geology 25:543–546

England PC, Thompson AB (1984) Pressure-temperature-time paths of regional metamorphism I. Heat transfer during the evolution of regions of thickened continental crust. J Petrol 25:894–928

Ferry JM, Watson EB (2007) New thermodynamic models and revised calibrations for the Ti-in-zircon and Zr-in-rutile thermometers. Contrib Mineral Petrol 154:429–437

Fu B, Page FZ, Cavosie AJ, Fournelle J, Kita NT, Lackey JS, Wilde SA, Valley JW (2008) Ti-in-zircon thermometry: applications and limitations. Contrib Mineral Petrol 156:197–215

Gaetani M, Garzanti E (1991) Multicyclic history of the northern India continental margin (northwestern Himalaya). Am Assoc Petroleum Geol Bull 75:1427–1446

Gansser A (1964) Geology of the Himalayas, 289. New York, NY

Gansser A (1983) Geology of the Bhutan Himalaya, 181. Birkäuser, Basel

Garzanti E (1999) Stratigraphy and sedimentary history of the Nepal Tethys Himalaya passive Margin. J Asian Earth Sci 17:805–827

Gehrels GE, DeCelles PG, Martin A et al (2003) Initiation of the Himalayan Orogen as an early Paleozoic thin skinned thrust belt. Geol Soc Am Today 13:4–9. doi:10.1130/1052-5173(2003)13<4:IOTHOA>2.0.CO;2

Godin L, Parrish RR, Brown RL, Hodges KV (2001) Crustal thickening leading to exhumation of the Himalayan Metamorphic core of central Nepal: insight from U–Pb Geochronology and Ar-40/Ar-39 Thermochronology. Tectonics 20:729–747

Groppo C, Lombardo B, Rolfo F, Pertusati P (2007) Clockwise exhumation path of granulitized eclogites from the Ama Drime range (eastern Himalayas). J Metamorph Geol 25:51–75

Grujic D, Casey M, Davidson C et al (1996) Ductile extrusion of the Higher Himalayan Crystalline in Bhutan: evidence from quartz microfabrics. Tectonophysics 260:21–43

Grujic D, Hollister LS, Parrish RP (2002) Himalayan metamorphic sequence as an orogenic channel: insight from Bhutan. Earth Plan Sci Lett 198:177–191

Grujic D, Warren CJ, Wooden JL (2011) Rapid synconvergent exhumation of Miocene-aged lower and orogenic crust in the eastern Himalaya. Lithosphere 3:346–366. doi:10.1130/L154.1

Harrison TM, Ryerson FJ, LeFort P, Yin A, Lovera O, Catlos EJ (1997) A late Miocene-Pliocene origin for the central Himalayan inverted metamorphism. Earth Plan Sci Lett. 146:E1–E7

Harrison TM, Grove M, Lovera OM, Catlos EJ (1998) A model for the origin of Himalayan anatexis and inverted metamorphism. J Geophys Res 103:27017–27032

Harrison TM, Celerier J, Aikman AB, Hermann J, Heizler MT (2009) Diffusion of ^{40}Ar in muscovite. Geochim et Cosmochim Acta 73:1039–1051. doi:10.1016/j.gca.2008.09.038

Heim A, Gansser A (1939) Central Himalaya: geological observations of the Swiss expedition, 1936. Mem Swiss Soc Nat Sci 73:245

Hermann J, Rubatto D (2003) Relating zircon and monazite domains to garnet growth zones: age and duration of granulite facies metamorphism in the Val Malenco lower crust. J Metamorph Geol 21:833–852

Hodges KV (2000) Tectonics of the Himalaya and southern Tibet from two perspectives. Geol Soc Am Bull 112:324–350

Hodges KV, Parrish RR, Searle MP (1996) Tectonic evolution of the central Annapurna Range, Nepalese Himalayas. Tectonics 15:1264–1291

Hollister LS, Grujic D (2006) Pulsed channel flow in Bhutan. Geol Soc Spec. Pubs. 268:415–423. doi:10.1144/GSL.SP.2006.268.01.19

Huyghe P, Mugnier JL, Gajurel AP, Delcaillau B (2005) Tectonic and climatic control of the changes in the sedimentary record of the Karnali River section (Siwaliks of western Nepal). The Island Arc 14:311–327

Jamieson RA, Beaumont C, Medvedev S, Nguyen MH (2004) Crustal channel flows: 2. Numerical models with implications for metamorphism in the Himalayan-Tibetan orogen: J Geophys Res 109:B06407. doi:10.1029/2003JB002811

Jamieson RA, Unsworth MJ, Harris NBW (2011) Crustal melting and the flow of mountains. Elements 7:253–260

Kellett DA, Grujic D, Erdmann S (2009) Miocene structural reorganization of the South Tibetan detachment, eastern Himalaya: implications for continental collision. Lithosphere 1:259–281. doi:10.1130/L56.1

Kellett DA, Grujic D, Warren CJ et al (2010) Metamorphic history of a syn-convergent orogen-parallel detachment: the South Tibetan detachment system, Bhutan Himalaya. J Metamorph Geol 28:785–808. doi:10.1111/j.1525-1314.2010.00893.x

Kelsey DE, Clark C, Hand M (2008) Thermobarometric modeling of zircon and monazite growth in melt-bearing systems: examples using model metapelitic and metapsammitic granulites. J Metam Geol. 26:199–212. doi:10.1111/j.1525-1314.2007.00757.x

Kohn MJ (2008) P-T-t data from central Nepal support critical taper and repudiate large-scale channel flow of the Greater Himalayan Sequence. Geol Soc Am Bull 120:259–273. doi:10.1016/j.gca.2008.05.045

Kohn MJ, Wieland MS, Parkinson CD, Upreti BN (2005) Five generations of monazite in Langtang gneisses; implications for chronology of the Himalayan metamorphic core. J Metamorph Geol 23:399–406. doi:10.1111/j.1525-1314.2005.00584.x

Kohn MJ, Paul SK, Corrie SL (2010) The lower Lesser Himalayan Sequence: a Paleoproterozoic arc on the northern margin of the Indian Plate. Geol Soc Am Bull 122:323–335. doi:10.1130/B26587.1

Kylander-Clark ARC, Hacker BR, Cottle JM (2013) Laser-ablation split-stream ICP petrochronology. Chem Geol 345:99–112. doi:10.1016/j.chemgeo.2013.02.019

Leech ML, Singh S, Jain AK et al (2005) The onset of India-Asia continental collision: early, steep subduction required by the timing of UHP metamorphism in the western Himalaya. Earth Planet Sci Lett 234:83–97. doi:10.1016/j.epsl.2005.02.038

LeFort P (1975) Himalayas: the collided range, present knowledge of the continental arc. Am J Sci 275-A:1–44

Long S, McQuarrie N (2010) Placing limits on channel flow: insights from the Bhutan Himalaya. Earth Planet Sci Lett 290:375–390. doi:10.1016/j.epsl.2009.12.033

Long S, McQuarrie N, Tobgay T et al (2011a) Tectonostratigraphy of the Lesser Himalaya of Bhutan: implications for the along-strike stratigraphic continuity of the northern Indian margin. Geol Soc Am Bull 123:1406–1426. doi:10.1130/B30202.1

Long S, McQuarrie N, Tobgay T, Grujic D (2011b) Geometry and crustal shortening of the Himalayan fold–thrust belt, eastern and central Bhutan. Geol Soc Am Bull 123:1427–1447. doi:10.1130/B30203.1

Long SP, McQuarrie N, Tobgay T et al (2011c) Geologic map of Bhutan. J Maps. doi:10.4113/jom.2011.1159

Long SP, McQuarrie N, Tobgay T et al (2012) Variable shortening rates in the eastern Himalayan thrust belt, Bhutan: insights from multiple thermochronologic and geochronologic datasets tied to kinematic reconstructions. Tectonics 31:TC5004. doi:10.1029/2012TC003155

Ludwig KR (2010) User's manual for Isoplot/Ex version 3.75: a geochronological toolkit for Microsoft Excel. Berkeley Geochronological Center, Spec. Pubs, Berkeley

Maluski H, Matte P, Brunel M (1988) Argon 39–Argon 40 dating of metamorphic and plutonic events in the north and high Himalaya belts (southern Tibet–China). Tectonics 7:299–326

Martin AJ, Burgy KD, Kaufman AJ, Gehrels GE (2011) Stratigraphic and tectonic implications of field and isotopic constraints on depositional ages of Proterozoic Lesser Himalayan rocks in central Nepal. Precambrian Res 185:1–17. doi:10.1016/j.precamres.2010.11.003

Mathew G, De Sarkar S, Pande K, Dutta S, Ali S, Rai A, Netrawali S (2013) Thermal metamorphism of the Arunachal Himalaya, India: raman thermometry and thermochronological constraints on the tectono-thermal evolution. Int J Earth Sci 102:1911–1936

Mattauer M (1986) Intracontinental subduction, crust-mantle decollement and crustal-stacking wedge in the Himalayas and other collision belts, in Coward MP, Ries AC (eds.). Geol Soc Am Spec Publ 19:37–50

McDonough W, Sun S (1995) The composition of the Earth. Chem Geol 254:223–253

McLean NM, Bowring JF, Bowring SA (2011) An algorithm for U–Pb isotope dilution data reduction and uncertainty propagation. Geochem Geophys Geosyst 12:Q0AA18. doi:10.1029/2010GC003478

McQuarrie N, Long SP, Tobgay T et al (2013) Documenting basin scale, geometry, and provenance through detrital geochemical data: lesson from the Neoproterozoic to Ordovician Lesser, Greater, and Tethyan Himalayan strata of Bhutan. Gondwana Res 23:1491–1510. doi:10.1016/j.gr.2012.09.002

Miller C, Thoni M, Frank W (2001) The early Palaeozoic magmatic event in the northwest Himalaya, India: source, tectonic setting and age of emplacement. Geol Mag 138:237–251

Mitra G, Bhattacharyya K, Mukul M (2010) The Lesser Himalayan duplex in Sikkim: implications for variations in Himalayan shortening. J Geol Soc India 75:276–288

Molnar P (1984) Structure and tectonics of the Himalaya: constraints and implications of geophysical data. Annu Rev Earth Planet Sci 12:489–518

Myrow PM, Hughes NC, Searle MP, Fanning CM, Peng S-C, Parcha SK (2009) Stratigraphic correlation of Cambrian–Ordovician deposits along the Himalaya: implications for the age and nature of rocks in the Mount Everest region. Geol Soc Am Bull 120:323–332. doi:10.1130/B26384.1

Myrow PM, Hughes NC, Goodge JW et al (2010) Extraordinary transport and mixing of sediment across Himalayan central Gondwana during the Cambrian-Ordovician. Geol Soc Am Bull 122:1660–1670. doi:10.1130/B30123.1

Najman Y, Appel E, Boudagher-Fadelm M et al (2010) Timing of India–Asia collision: geological, biostratigraphic, and palaeomagnetic constraints. J Geophys Res 115:B1241. doi:10.1029/2010JB007673

Parrish RR, Hodges KV (1996) Isotopic constraints on the age and provenance of the Lesser and Greater Himalayan sequences, Nepalese Himalaya. Geol Soc Am Bull 108:904–911

Pyle JM, Spear FS (2003) Four generations of accessory-phase growth in low-pressure migmatites from SW New Hampshire. Am Min 88:338–351

Robinson DM, DeCelles PG, Copeland P (2006) Tectonic evolution of the Himalayan thrust belt in western Nepal: implications for channel flow models. Geol Soc Am Bull 118:865–885

Rosenberg CL, Handy MR (2005) Experimental deformation of partially melted granite revisited: implications for the continental crust. J Metamorph Geol 23:19–28. doi:10.1111/j.1525-1314.2005.00555.x

Rowley DB (1996) Age of collision between India and Asia: a review of the stratigraphic data. Earth Planet Sci Lett 145:1–13

Royden LH, Burchfiel BC, King RW, Wang E, Chen Z, Shen F, Liu Y (1997) Surface deformation and lower crustal flow in eastern Tibet. Science 276:788–790

Rubatto D (2002) Zircon trace-element geochemistry: partitioning with garnet and the link between U–Pb ages and metamorphism. Chem Geol 184:123–138

Rubatto D, Hermann J (2007) Experimental zircon/melt and zircon/garnet trace element partitioning and implications for the geochronology of crustal rocks. Chem Geol 241:62–87

Rubatto D, Chakraborty S, Dasgupta S (2013) Timescales of crustal melting in the Higher Himalayan Crystallines (Sikkim, Eastern Himalaya) inferred from trace element-constrained monazite and zircon chronology. Contrib Mineral Petrol 165:349–372. doi:10.1007/s00410-012-0812-y

Schärer U (1984) The effect of initial ^{230}Th disequilibrium on young U–Pb ages: the Makalu case, Himalaya. Earth Planet Sci Lett 67:191–204

Schelling D, Arita K (1991a) Thrust tectonics, crustal shortening, and the structure of the far-eastern Nepal Himalaya. Tectonics 10:851–862

Schelling D, Arita K (1991b) Thrust tectonics, crustal shortening, and the structure of the far-eastern Nepal Himalaya. Tectonics 10:851–862

Spear FS, Kohn MJ, Cheney JT (1999) P–T paths from anatectic pelites. Contrib Mineral Petrol 134:17–32

Srivastava P, Mitra G (1994) Thrust geometries and deep structure of the outer and lesser Himalaya, Kumaon and Garwal (India): implications for evolution of the Himalayan fold-and-thrust belt. Tectonics 13:89–109

Stearns MA, Hacker BR, Ratschbacher L, Lee J, Cottle JM, Kylander-Clark A (2013) Synchronous Oligocene–Miocene metamorphism of the Pamir and the north Himalaya driven by plate-scale dynamics. Geology. doi:10.1130/G34451.1

Stüwe K, Foster D (2001) 40Ar/39Ar, pressure, temperature and fission track constraints on the age and nature of metamorphism around the Main Central Thrust in the eastern Bhutan Himalaya. J Asian Earth Sci 19:85–95. doi:10.1016/S1367-9120(00)00018-3

Swapp SM, Hollister LS (1991) Inverted metamorphism within the Tibetan slab of Bhutan: evidence for a tectonically transported heat source. Can Mineral 29:1019–1041

Tobgay T, McQuarrie N, Long SP et al (2012) The age and rate of displacement along the Main Central Thrust in the western Bhutan Himalaya. Earth Planet Sci Lett 319–320:146–158. doi:10.1016/j.epsl.2011.12.005

Torvela T, Moreau J, Butler RWH, Korja A, Heikkinen P (2013) The mode of deformation in the orogenic mid-crust revealed by seismic attribute analysis. Geochem Geophys Geosyst 14:1069–1086

Vanderhaeghe O, Teyssier T (2001) Partial melting and flow of orogens. Tectonophysics 342:451–472

Vannay JC, Hodges K (1996) Tectonometamorphic evolution of the Himalayan metamorphic core between Annapurna and Dhaulagiri, central Nepal. J Metamorph Geol 14:635–656. doi:10.1046/j.1525-1314.1996.00426.x

Vermeesch P (2012) On the visualization of detrital age distributions. Chem Geol 312–313:190–194. doi:10.1016/j.chemgeo.2012.04.021

Warren CJ, Grujic D, Cottle JM, Rogers NW (2011a) Constraining cooling histories: rutile and titanite chronology and diffusion modeling in NW Bhutan. J Meta Geol. doi:10.1111/j.1525-1314.2011.00958.x

Warren CJ, Grujic D, Kellett DA et al (2011b) Probing the depths of the India–Asia collision: U–Th–Pb monazite chronology of granulites from NW Bhutan. Tectonics 30:TC2004. doi:10.1029/2010TC002738

Warren CJ, Singh AK, Roberts NMW, Regis D, Halton AM, Singh RB (2014) Timing and conditions of peak metamorphism and cooling across the Zimithang Thrust, Arunachal Pradesh, India. Lithos 200–201:94–110. doi:10.1016/j.lithos.2014.04.005

Watson EB, Wark DA, Thomas JB (2006) Crystallization thermometers for zircon and rutile. Contrib Mineral Petrol 151:413–433

Wei CJ, Powell R, Clarke GL (2004) Calculated phase equilibria for low- and medium-pressure metapelites in the KFMASH and KMnFMASH systems. J Metamorph Geol 22:495–508

Whitney DL, Evans BW (2010) Abbreviations for names of rock-forming minerals. Am Min 95:185–187

Wu C, Nelson KD, Wortman G, Samson SD, Yue Y, Li J, Kidd SF, Edwards MA (1998) Yadong cross structure and South Tibetan Detachment in the east central Himalaya (89°–90°E). Tectonics 17:28–45

Yin A (2006) Cenozoic tectonic evolution of the Himalayan orogen as constrained by along-strike variation of structural geometry, exhumation history, and foreland sedimentation. Earth Sci Rev 76:1–131. doi:10.1016/j.earscirev.2005.05.004

Yin A, Harrison TM (2000) Geologic evolution of the Himalayan-Tibetan orogen. Ann Rev Earth Plan Sci 28:211–280

Yin A, Dubey C, Kelty T et al (2006) Structural evolution of the Arunachal Himalaya and implications for asymmetric development of the Himalayan orogen. Current Science-Bangalore 90:195–206

Yin A, Dubey C, Webb A et al (2010a) Geologic correlation of the Himalayan orogen and Indian craton: part 1. Structural geology, U–Pb zircon geochronology, and tectonic evolution of the Shillong Plateau and its neighboring regions in NE India. Geol Soc Am Bull 122:336–359. doi:10.1130/B26460.1

Yin A, Dubey C, Kelty T, Webb A, Harrison T, Chou C, Célérier J (2010b) Geologic correlation of the Himalayan orogen and Indian craton: part 2. Structural geology, geochronology, and tectonic evolution of the eastern Himalaya. Geol Soc Am Bull 122:360–395